Journal of Computational Physics 235 (2013) 423–445

Contents lists available at SciVerse ScienceDirect

Journal of Computational Physics

journal homepage: www.elsevier.com/locate/jcp

Numerical methods and comparison for computing dark and bright solitons in the nonlinear Schrödinger equation

Weizhu Bao [a,*], Qinglin Tang [a], Zhiguo Xu [b]

[a] Department of Mathematics and Center for Computational Science and Engineering, National University of Singapore, Singapore 119076, Singapore
[b] Beijing Computational Science Research Center, Beijing 100084, PR China

ARTICLE INFO

Article history:
Received 13 April 2012
Received in revised form 13 October 2012
Accepted 26 October 2012
Available online 23 November 2012

Keywords:
Nonlinear Schrödinger equation
Dark soliton
Bright soliton
Finite difference method
Spectral method
Time splitting

ABSTRACT

In this paper, we propose new efficient and accurate numerical methods for computing dark solitons and review some existing numerical methods for bright and/or dark solitons in the nonlinear Schrödinger equation (NLSE), and compare them numerically in terms of accuracy and efficiency. We begin with a review of dark and bright solitons of NLSE with defocusing and focusing cubic nonlinearities, respectively. For computing dark solitons, to overcome the nonzero and/or non-rest (or highly oscillatory) phase background at far field, we design efficient and accurate numerical methods based on accurate and simple artificial boundary conditions or a proper transformation to rest the highly oscillatory phase background. Stability and conservation laws of these numerical methods are analyzed. For computing interactions between dark and bright solitons, we compare the efficiency and accuracy of the above numerical methods and different existing numerical methods for computing bright solitons of NLSE, and identify the most efficient and accurate numerical methods for computing dark and bright solitons as well as their interactions in NLSE. These numerical methods are applied to study numerically the stability and interactions of dark and bright solitons in NLSE. Finally, they are extended to solve NLSE with general nonlinearity and/or external potential and coupled NLSEs with vector solitons.

1. Introduction

Solitons are those self-reinforcing solitary waves with notable stability properties that keep their shapes and velocity during propagation. They arise in many areas of physics such as the optical fiber communications, hydrodynamics, solid state physics, biological physics and atomic physics [1,21]. Since they were first observed and described by Russell [34], many fascinating experiments and remarkable mathematical theories have been developed to describe and study their properties [21,32]. In this paper, we consider the soliton dynamics in the nonlinear Schrödinger equation (NLSE) in one dimension (1D) with cubic nonlinearity, which is a completely integrable system [43,44,33]:

$$i\partial_t\psi(x,t) = -\frac{1}{2}\partial_{xx}\psi(x,t) + \beta|\psi(x,t)|^2\psi(x,t), \quad x \in \mathbb{R}, \quad t > 0, \tag{1.1}$$

where t is time, x is spatial coordinate, ψ is a complex-valued wave function or order parameter, and β is a dimensionless constant with positive value for defocusing (or repulsive) and negative value for focusing (or attractive) nonlinearity,

* Corresponding author.
E-mail addresses: bao@math.nus.edu.sg, bao@cz3.nus.edu.sg (W. Bao), tqltql2010@gmail.com (Q. Tang), xuzg11@csrc.ac.cn (Z. Xu).
URL: http://www.math.nus.edu.sg/bao/ (W. Bao).

0021-9991/$ - see front matter © 2012 Elsevier Inc. All rights reserved.
http://dx.doi.org/10.1016/j.jcp.2012.10.054

respectively. Among the seas of conserved quantities of this equation, the three important ones are the *normalization* of the wave function

$$N(t) := N(\psi(\cdot,t)) = \int_{\mathbb{R}} |\psi(x,t)|^2 dx, \quad t \geqslant 0, \tag{1.2}$$

the *momentum*

$$P(t) := P(\psi(\cdot,t)) = \frac{i}{2}\int_{\mathbb{R}} \left[\psi(x,t)\partial_x\bar{\psi}(x,t) - \bar{\psi}(x,t)\partial_x\psi(x,t)\right] dx, \quad t \geqslant 0, \tag{1.3}$$

where $\bar{\psi}$ denotes the complex conjugate of ψ, and the *energy*

$$E(t) := E(\psi(\cdot,t)) = \frac{1}{2}\int_{\mathbb{R}} \left[|\partial_x\psi(x,t)|^2 + \beta|\psi(x,t)|^4\right] dx, \quad t \geqslant 0. \tag{1.4}$$

The NLSE (1.1) has been widely used to successfully study solitons in dispersive nonlinear optical fibers [25,26,29], and for analyzing the properties of the matter-wave solitons [23,18,19] shortly after the realization of Bose–Einstein condensate [5]. In general, solitons are formed when the nonlinear term exactly balances the wave packet dispersion, and two different types of solitons, i.e. bright and dark solitons when $\beta < 0$ and $\beta > 0$, respectively, have been observed in experiments and widely studied in theories for the NLSE [43,44].

Bright solitons are of concave-shape density that can survive when the self-phase modulation balances the dispersion of the pulse in nonlinear optics and/or in a self-focusing media for the nonlinear matter waves. When $\beta < 0$, the NLSE (1.1) admits bright solitons in the following form [43,29]:

$$\psi_B(x,t) = \frac{a}{\sqrt{-\beta}}\operatorname{sech}(a(x - vt - x_0))e^{i(vx - \frac{1}{2}(v^2 - a^2)t + \theta_0)}, \quad x \in \mathbb{R}, \quad t \geqslant 0. \tag{1.5}$$

Here $\frac{a}{\sqrt{-\beta}}$ is the amplitude with a an arbitrary real constant, v is the velocity of the soliton, and x_0 and θ_0 are two real constants representing the shifts of the soliton in space and phase at $t = 0$, respectively. Due to the exponential decay of the above bright soliton solution when $|x| \to \infty$, the conserved quantities in (1.2)–(1.4) are well defined. In fact, plugging (1.5) into (1.2)–(1.4), when $\beta < 0$, we obtain

$$N(\psi_B) = \frac{2a}{-\beta}, \quad P(\psi_B) = \frac{2av}{-\beta}, \quad E(\psi_B) = \frac{av^2}{-\beta} + \frac{a^3}{-3\beta}, \tag{1.6}$$

which immediately imply the particle-like nature of the bright soliton [19] with: effective mass as $M_b = \frac{2a}{-\beta}$, effective momentum as $P_b = M_b v$, effective energy as $E_b = \frac{1}{2}M_b v^2 + \frac{1}{24}\beta^2 M_b^3 = \frac{1}{2M_b}P_b^2 + \frac{1}{24}\beta^2 M_b^3$, and $\frac{\partial E_b}{\partial P_b} = \frac{P_b}{M_b} = v$.

In addition, different numerical methods have been proposed for solving the dynamics of the NLSE (1.1) with the above bright soliton solutions and/or other related solutions which decay to zero when $|x| \to \infty$. In this case, the original problem is usually truncated on a bounded computational domain, e.g. an interval, with either simple boundary conditions such as homogeneous Dirichlet [3,20], or periodic [38,42], or homogeneous Neumann [35,24] boundary conditions; or complicated and high order boundary conditions such as transport boundary conditions [6,45,7,27]. When the bounded computational domain is chosen large enough, the approximation is usually very accurate. Then the truncated problem is usually discretized in space by either finite difference method [3,20,22,35,31,41], or spectral method [8,10,36,38], or finite element method [46]; and in time by either the conservative Crank–Nicolson method [22], or time splitting method [17,11,42], or semi-implicit method, or 4th-order Runge–Kutta method [3,4,28]. Based on these efficient and accurate numerical methods, the stability and interaction of the above bright solitons have been well and widely studied analytically and numerically as well as asymptotically in the literatures.

On the other hand, dark solitons are of convex-shape density with a non-trivial phase jump across the density minimum that can be supported in a defocusing media. When $\beta > 0$, the NLSE (1.1) admits dark solitons. By means of inverse scattering transform [2,29], dark solitons are in the form of [19,23,43,29]

$$\psi_D(x,t) = \left[\cos\phi\tanh\left(\sqrt{u_0\beta}\cos\phi(x - vt - x_0)\right) + i\sin\phi\right]\psi_{bg}(x,t), \tag{1.7}$$

which are living on the nonzero background

$$\psi_{bg}(x,t) = \sqrt{u_0}e^{i(kx - \omega t + \theta_0)}, \quad x \in \mathbb{R}, \quad t \geqslant 0, \tag{1.8}$$

where $u_0 > 0$ is a constant, x_0 and θ_0 are two real constants representing the shifts of the soliton in space and phase at $t = 0$, respectively, k and ω are the wave number and frequency of the background, respectively, satisfying the dispersion relation $\omega = \frac{1}{2}k^2 + \beta u_0$, v is the relative velocity between the soliton and the background given by $v = \sqrt{u_0\beta}\sin\phi + k$ with ϕ ($|\phi| < \frac{\pi}{2}$) the so called soliton phase angle describing the darkness of the soliton, namely

$$|\psi_D(x,t)|^2 = u_0[1 - \cos^2\phi\operatorname{sech}^2(\sqrt{u_0\beta}\cos\phi(x - vt - x_0))], \quad x \in \mathbb{R}, \quad t \geqslant 0. \tag{1.9}$$

In this way, the so called *black* and *gray* solitons correspond to the cases $\phi = 0$ and $\phi \neq 0$, respectively. Notice that there are two independent parameters u_0 and k for the background in the formula (1.8), it is naturally to divide the dark soliton solu-

tions into two groups according to the stationary of the background. If a dark soliton lives on a rest background, i.e. $k = 0$, we call it as type I dark soliton; otherwise, i.e. $k \neq 0$, we name it as type II dark soliton. By introducing $a = \sqrt{u_0\beta}\cos\phi$, the type I dark solitons can be reformulated as

$$\psi_{D1}(x,t) = \frac{1}{\sqrt{\beta}}[a\tanh(a(x - vt - x_0)) + iv]e^{i(-(a^2+v^2)t+\theta_0)}, \quad x \in \mathbb{R}, \quad t \geqslant 0, \tag{1.10}$$

and respectively, type II dark solitons can be reformulated as

$$\psi_{D2}(x,t) = \frac{1}{\sqrt{\beta}}[a\tanh(a(x - vt - x_0)) + i(v - k)]e^{i(kx-\frac{1}{2}[k^2+2a^2+2(v-k)^2]t+\theta_0)}. \tag{1.11}$$

Due to the nonzero and/or non-rest (or highly oscillatory) phase background of the above dark soliton solutions (1.7) when $|x| \to \infty$, the conserved quantities in (1.2)–(1.4) are not well defined. In fact, it is easy to check that $N(\psi_D) = \infty, P(\psi_D) = \infty$ and $E(\psi_D) = \infty$. Thus, for the dark soliton solutions (1.7) of the NLSE, one might need to renormalized the integrals in (1.2)–(1.4) to exclude the contribution of the background such that the new integrals are finite and reveal the particle-like nature of the dark solitons. For details, one can refer to [19,23,15,30,40] and references therein.

From the numerical point of view, it brings significant difficulties and numerical burden due to the appearance of nonzero and/or non-rest (or highly oscillatory) phase background at far field in the solutions of NLSE such as the dark soliton solutions (1.7). In this case, the original problem can still be truncated on a bounded computational domain. However, the simple boundary conditions such as homogeneous Dirichlet, or periodic, or homogeneous Neumann boundary conditions; and the complicated and high order boundary conditions such as transport boundary conditions are no longer valid. To our knowledge, there is not too much work on designing and comparing efficient and accurate numerical methods for solving NLSE with nonzero far field conditions, especially with non-rest (or highly oscillatory) phase background such as the type II dark solitons. Due to the realization of Bose–Einstein condensation, it has been more and more demanded to study theoretically the stability and interaction of dark solitons of NLSE [19,23,29,30,40]. The main aim of this paper is to present and compare efficient and accurate numerical methods for solving NLSE with nonzero far field conditions such as the dark soliton solutions. By designing accurate and simple artificial boundary conditions or introducing a proper transformation to rest the highly oscillatory phase background, we design different numerical methods for computing dark solitons in NLSE and compare their efficiency and accuracy as well as computational complexity. Comparison with different existing numerical methods for NLSE with solutions decay to zero when $|x| \to \infty$, such as the bright soliton solution, will also be carried out so as to identify the most efficient and accurate numerical methods for studying numerically the stability and interaction of dark and bright solitons of NLSE. To solve (1.1) numerically, we assume the following initial condition

$$\psi(x,0) = \psi_0(x), \quad x \in \mathbb{R}. \tag{1.12}$$

The rest of this paper is organized as follows. In Section 2, we propose numerical methods for solving NLSE with type II dark soltions and compare them numerically. Similar results for type I dark solitons and bright solitons of NLSE are presented in Sections 3 and 4, respectively. Extension to NLSE with general nonlinearity and/or external potential and the coupled NLSEs with vector solitons is given in Section 5. Finally, some conclusions are drawn in Section 6.

2. Numerical methods for NLSE with type II dark solitons

In this section, we will present new efficient and accurate numerical methods for the NLSE (1.1) with (1.12) when the solution admits type II dark soliton at far field, i.e. the solution has non-rest (or highly oscillatory) phase background at far field. Without loss of generality, e.g. type II dark soliton, we assume that the initial data ψ_0 satisfies

$$\psi_0(x) \to A_\pm^0 e^{ikx}, \quad x \to \pm\infty, \tag{2.1}$$

where $k \neq 0$ is a given real constant and $A_+^0 \neq A_-^0$ are two given complex constants. Under this far field assumption on the initial data, by using the disperison relation of the NLSE and the method of separation of variables, formally, we get the solution ψ of the NLSE (1.1) with (1.12) satisfies

$$\psi(x,t) \to A_\pm(t)e^{ikx}, \quad x \to \pm\infty, \quad t \geqslant 0. \tag{2.2}$$

Plugging (2.2) into (1.1), we obtain formally

$$iA'_\pm(t) = \frac{k^2}{2}A_\pm(t) + \beta|A_\pm(t)|^2A_\pm, \quad t > 0, \tag{2.3}$$

with initial condition $A_\pm(0) = A_\pm^0$. Multiplying (2.3) by the conjugate of $A_\pm(t)$ and then subtracting from its conjugate, we get for $\rho_\pm(t) := |A_\pm(t)|^2$ as

$$\rho'_\pm(t) \equiv 0, \quad t > 0,$$

which immediately implies that

$$\rho_\pm(t) \equiv \rho_\pm(0) = |A_\pm^0|^2, \quad t \geqslant 0.$$

Plugging it into (2.3) and solving it analytically, we get

$$\psi(x,t) \to A_\pm^0 e^{-i(k^2+2\beta|A_\pm^0|^2)t/2} e^{ikx}, \quad x \to \pm\infty, \quad t \geqslant 0. \tag{2.4}$$

This implies that the solution $\psi(x,t)$ of the NLSE (1.1) with (1.12) has the same oscillatory phase background at far field in space as that in its initial data $\psi_0(x)$.

2.1. Numerical methods based on accurate and simple boundary conditions

Based on the far field asymptotic behavior (2.4) of the solution ψ, differentiating (2.4) with respect to x, we get

$$\partial_x\psi(x,t) - ik\psi(x,t) \to 0, \quad x \to \pm\infty, \quad t \geqslant 0. \tag{2.5}$$

This immediately provides an accurate and simple far field condition for the solution ψ. In fact, by choosing an interval $\Omega = [L_1, L_2]$ properly and large enough, the original problem (1.1) with (1.12) can be approximated by

$$i\partial_t\psi(x,t) = -\frac{1}{2}\partial_{xx}\psi(x,t) + \beta|\psi(x,t)|^2\psi(x,t), \quad L_1 < x < L_2, \quad t > 0, \tag{2.6}$$

$$\partial_x\psi(L_1,t) - ik\psi(L_1,t) = \partial_x\psi(L_2,t) - ik\psi(L_2,t) = 0, \quad t > 0, \tag{2.7}$$

$$\psi(x,0) = \psi_0(x), \quad L_1 \leqslant x \leqslant L_2. \tag{2.8}$$

For the above problem, we can define the modified *mass* and *energy* as

$$N_1(t) := \int_{L_1}^{L_2} |\psi(x,t)|^2 dx + k\int_0^t (|\psi(L_2,s)|^2 - |\psi(L_1,s)|^2) ds, \quad t \geqslant 0, \tag{2.9}$$

$$E_1(t) := \frac{1}{2}\int_{L_1}^{L_2} (|\partial_x\psi|^2 + \beta|\psi|^4) dx + k\mathrm{Im}\int_0^t \left[\psi(L_2,s)\partial_s\bar{\psi}(L_2,s) - \psi(L_1,s)\partial_s\bar{\psi}(L_1,s)\right] ds, \tag{2.10}$$

where $\bar{f}$ and Im (f) denote the conjugate and imaginary part of f, respectively. Then we can prove that the modified mass and energy are conserved (see detailed proof in Appendix A):

Lemma 2.1. *The truncated problem (2.6)–(2.8) conserves the modified mass (2.9) and energy (2.10), i.e.*

$$N_1(t) \equiv N_1(0) = \int_{L_1}^{L_2} |\psi_0(x)|^2 dx, \quad E_1(t) \equiv E_1(0) = \frac{1}{2}\int_{L_1}^{L_2} (|\partial_x\psi_0|^2 + \beta|\psi_0|^4) dx, \quad t \geqslant 0. \tag{2.11}$$

In order to present numerical methods for discretizing the problem (2.6)–(2.8), we choose time step $\tau > 0$ and mesh size $h = (L_2 - L_1)/N$ with N an even positive integer, denote the grid points and time steps as

$$x_j := L_1 + jh, \quad j = 0, \ldots, N; \quad t_n := n\tau, \quad n = 0, 1, \ldots.$$

Let ψ_j^n be the numerical approximation of $\psi(x_j, t_n)$ $(j = 0, 1, \ldots, N,\ n = 0, 1, \ldots)$ and introduce the finite difference operators

$$\delta_t^+\psi_j^n = \frac{\psi_j^{n+1} - \psi_j^n}{\tau}, \quad \delta_t\psi_j^n = \frac{\psi_j^{n+1} - \psi_j^{n-1}}{2\tau}, \quad \delta_x^-\psi_j^n = \frac{\psi_j^n - \psi_{j-1}^n}{h},$$
$$\delta_x^+\psi_j^n = \frac{\psi_{j+1}^n - \psi_j^n}{h}, \quad \delta_x\psi_j^n = \frac{\psi_{j+1}^n - \psi_{j-1}^n}{2h}, \quad \delta_x^2\psi_j^n = \frac{\psi_{j+1}^n - 2\psi_j^n + \psi_{j-1}^n}{h^2}.$$

We will consider two finite difference methods for discretizing the problem (2.6)–(2.8). The first one is conservative Crank–Nicolson finite difference (CNFD) method in which the Crank–Nicolson scheme is applied for temporal derivative and second-order central finite difference is applied for spatial derivatives:

$$i\delta_t^+\psi_j^n = -\frac{1}{4}\delta_x^2(\psi_j^{n+1} + \psi_j^n) + \frac{\beta}{4}(|\psi_j^{n+1}|^2 + |\psi_j^n|^2)(\psi_j^{n+1} + \psi_j^n), \quad 0 \leqslant j \leqslant N, \quad n \geqslant 0. \tag{2.12}$$

The boundary condition (2.7) is discretized as:

$$\frac{\psi_1^{n+1} - \psi_{-1}^{n+1}}{2h} - ik\psi_0^{n+1} = 0, \quad \frac{\psi_{N+1}^{n+1} - \psi_{N-1}^{n+1}}{2h} - ik\psi_N^{n+1} = 0, \quad n \geqslant 0, \tag{2.13}$$

and the initial condition (2.8) is discretized as:

$$\psi_j^0 = \psi_0(x_j), \quad j = 0, 1, \ldots, N. \tag{2.14}$$

In this CNFD method, at every time step, one needs to solve a fully nonlinear coupled system which is time consuming. Thus, in practical computation, the Crank–Nicolson scheme for temporal derivative in (2.12) is replaced by the Crank–Nicolson/leap-frog scheme for temporal derivative with respect to linear/nonlinear terms and it is usually called as semi-implicit finite difference (SIFD) method:

$$i\delta_t\psi_j^n = -\frac{1}{4}\delta_x^2(\psi_j^{n+1}+\psi_j^{n-1}) + \beta|\psi_j^n|^2\psi_j^n, \quad 0 \leqslant j \leqslant N, \quad n \geqslant 1. \tag{2.15}$$

Define the mass and energy in the discrete level as

$$N_1^n := \frac{h}{2}\sum_{j=0}^{N-1}\left(|\psi_j^n|^2 + |\psi_{j+1}^n|^2\right) + k\tau\sum_{l=1}^{n}\left(|\psi_N^{l-\frac{1}{2}}|^2 - |\psi_0^{l-\frac{1}{2}}|^2\right), \quad n \geqslant 0, \tag{2.16}$$

$$E_1^n := \frac{h}{2}\sum_{j=0}^{N-1}\left[|\delta_x^+\psi_j^n|^2 + \frac{\beta}{2}\left(|\psi_j^n|^4 + |\psi_{j+1}^n|^4\right)\right] + k\tau\mathrm{Im}\sum_{l=1}^{n}\left[\psi_N^{l-\frac{1}{2}}\delta_t^+\bar{\psi}_N^{l-1} - \psi_0^{l-\frac{1}{2}}\delta_t^+\bar{\psi}_0^{l-1}\right], \tag{2.17}$$

respectively, where $\psi_j^{l+1/2} = \frac{1}{2}(\psi_j^{l+1} + \psi_j^l)$. Then for the CNFD method (2.12)–(2.14), we can prove that the mass and energy are conserved in the discrete level (see detailed proof in Appendix B):

Lemma 2.2. *The CNFD method (2.12)–(2.14) conserves the mass and energy in the discrete level, i.e.*

$$N_1^n \equiv N_1^0, \quad E_1^n \equiv E_1^0, \quad n \geqslant 0. \tag{2.18}$$

It is easy to see that both CNFD and SIFD methods are implicit, time symmetric, second order in both space and time, and the memory cost is $O(N)$. The CNFD method is unconditionally stable and it conserves the mass and energy in the discrete level, however, it needs to solve a fully nonlinear coupled system at every time step which might be tedious in programming and time consuming in practical computation. The SIFD method is conditionally stable under the stability condition $\tau \leqslant 1/(|\beta|\max_{0\leqslant j\leqslant N,\ n\geqslant 0}|\psi_j^n|^2)$ and it needs only to solve a linear coupled system which can be solved very efficiently via Thomas algorithm, thus it is efficient and easy to program and the computational cost per time step is $O(N)$.

2.2. Numerical methods based on a transformation

Based on the far field asymptotic behavior (2.4) of the solution ψ, we introduce the following transformation to 'rest' the highly oscillatory phase background at far field:

$$\phi(x,t) = \psi(x,t)e^{-ikx} \Longleftrightarrow \psi(x,t) = \phi(x,t)e^{ikx}, \quad x \in \mathbb{R}, \quad t \geqslant 0. \tag{2.19}$$

Then we have

$$\phi(x,t) \to A_\pm^0 e^{-i(k^2+2\beta|A_\pm^0|^2)t/2} \Rightarrow \partial_x\phi(x,t) \to 0, \quad x \to \pm\infty, \quad t \geqslant 0. \tag{2.20}$$

Plug (2.19) into (1.1) and notice (2.20), the original problem can be truncated and approximated as

$$i\partial_t\phi(x,t) = -\frac{1}{2}\partial_{xx}\phi - ik\partial_x\phi + \frac{1}{2}k^2\phi + \beta|\phi|^2\phi, \quad L_1 < x < L_2, \quad t > 0, \tag{2.21}$$

$$\partial_x\phi(L_1,t) = \partial_x\phi(L_2,t) = 0, \quad t > 0, \tag{2.22}$$

$$\phi(x,0) = \phi_0(x) := \psi_0(x)e^{-ikx}, \quad L_1 \leqslant x \leqslant L_2. \tag{2.23}$$

For this truncated problem, we can define the modified *mass* and *energy* as

$$N_2(t) := \int_{L_1}^{L_2}|\phi(\mathbf{x},t)|^2d\mathbf{x} + k\int_0^t(|\phi(L_2,s)|^2 - |\phi(L_1,s)|^2)ds, \tag{2.24}$$

$$E_2(t) := \frac{1}{2}\int_{L_1}^{L_2}\left[|\partial_x\phi|^2 + k^2|\phi|^2 - 2k\mathrm{Im}(\phi\partial_x\bar{\phi}) + \beta|\phi|^4\right]dx + k\mathrm{Im}\int_0^t\left[\phi(L_2,s)\partial_s\bar{\phi}(L_2,s) - \phi(L_1,s)\partial_s\bar{\phi}(L_1,s)\right]ds, \quad t \geqslant 0. \tag{2.25}$$

Then similar to the proof of Lemma 2.1, we can prove that the modified mass and energy are conserved:

Lemma 2.3. *The truncated problem (2.21)–(2.23) conserves the energy and mass defined above, i.e.*

$$N_2(t) \equiv N_2(0), \quad E_2(t) \equiv E_2(0), \quad t \geqslant 0. \tag{2.26}$$

Denote ϕ_j^n be the numerical approximation of $\phi(x_j,t_n)$, then a numerical approximation of $\psi(x_j,t_n)$ to the problem (2.6)–(2.8) is:

$$\psi_j^n = \phi_j^n e^{ikx_j}, \quad j = 0, 1, \ldots, N, \quad n = 0, 1, \ldots. \tag{2.27}$$

Applying the conservative Crank–Nicolson finite difference discretization to the problem (2.21)–(2.23), we obtain a conservative Crank–Nicolson finite difference through the transformation (2.27) (CNFD-T) to the original problem as

$$i\delta_t^+ \phi_j^n = -\frac{1}{2}\left(\delta_x^2 + 2ik\delta_x - k^2\right)\phi_j^{n+\frac{1}{2}} + \frac{\beta}{2}(|\phi_j^{n+1}|^2 + |\phi_j^n|^2)\phi_j^{n+\frac{1}{2}}, \quad 0 \leqslant j \leqslant N, \quad n \geqslant 0, \tag{2.28}$$

where $\phi_j^{n+\frac{1}{2}} = \frac{1}{2}(\phi_j^{n+1} + \phi_j^n)$. The boundary condition (2.22) is discretized as:

$$\frac{\phi_1^{n+1} - \phi_{-1}^{n+1}}{2h} = 0, \quad \frac{\phi_{N+1}^{n+1} - \phi_{N-1}^{n+1}}{2h} = 0, \quad n \geqslant 0, \tag{2.29}$$

and the initial condition (2.23) is discretized as:

$$\phi_j^0 = \phi_0(x_j) = \psi_0(x_j)e^{-ikx_j}, \quad j = 0, 1, \ldots, N. \tag{2.30}$$

Similarly, the above CNFD-T discretization (2.28) can be replaced by the following semi-implicit finite difference through the transformation (2.27) (SIFD-T) to the original problem as

$$i\delta_t \phi_j^n = -\frac{1}{4}\left(\delta_x^2 + 2ik\delta_x - k^2\right)[\phi_j^{n+1} + \phi_j^{n-1}] + \beta|\phi_j^n|^2\phi_j^n, \quad 0 \leqslant j \leqslant N, \quad n \geqslant 1. \tag{2.31}$$

In addition, due to the homogeneous Neumann boundary condition (2.22), the problem (2.21)–(2.23) can also be discretized by the following time-splitting finite difference (TSFD) method in which a time-splitting technique is applied first to decouple the nonlinearity and then a Crank–Nicolson finite difference is applied to discretize a linear Schrödinger equation. From time $t = t_n$ to $t = t_{n+1}$, we first solve

$$i\partial_t \phi(x,t) = \frac{1}{2}\left[k^2 + 2\beta|\phi(x,t)|^2\right]\phi(x,t), \quad L_1 \leqslant x \leqslant L_2, \quad t \geqslant t_n, \tag{2.32}$$

for time step of length τ, and then solve

$$\begin{cases} i\partial_t \phi(x,t) = -\frac{1}{2}\partial_{xx}\phi(x,t) - ik\partial_x\phi(x,t), & L_1 < x < L_2, \quad t > t_n, \\ \partial_x\phi(L_1,t) = \partial_x\phi(L_2,t) = 0, & t \geqslant t_n, \end{cases} \tag{2.33}$$

for the same time step τ. In (2.32), it leaves the density $\rho(x,t) := |\phi(x,t)|^2$ unchanged [11], i.e. $\rho(x,t) = \rho(x,t_n)$ for $t \geqslant t_n$ and thus it can be solved analytically as [11]

$$\phi(x,t) = e^{-i(t-t_n)(k^2+2\beta|\phi(x,t_n)|^2)/2}\phi(x,t_n), \quad L_1 \leqslant x \leqslant L_2, \quad t \geqslant t_n.$$

The linear Schrödinger equation (2.33) can be discretized by the CNFD method. By combining the time-splitting via the second-order Strang splitting [37], we obtain a time-splitting finite difference through the transformation (2.27) (TSFD-T) to the original problem as

$$\begin{cases} \phi_j^{(1)} = e^{-i\tau(k^2+2\beta|\phi_j^n|^2)/4}\phi_j^n, \\ i\frac{\phi_j^{(2)} - \phi_j^{(1)}}{\tau} = -\frac{1}{4}(\delta_x^2 + 2ik\delta_x)[\phi_j^{(2)} + \phi_j^{(1)}], \quad 0 \leqslant j \leqslant N, \quad n \geqslant 0, \\ \phi_j^{n+1} = e^{-i\tau(k^2+2\beta|\phi_j^{(2)}|^2)/4}\phi_j^{(2)}, \end{cases} \tag{2.34}$$

with the boundary conditions for the middle step as

$$\phi_{-1}^{(2)} = \phi_1^{(2)}, \quad \phi_{N+1}^{(2)} = \phi_{N-1}^{(2)}. \tag{2.35}$$

Again, define the mass and energy in the discrete level as

$$N_2^n := \frac{h}{2}\sum_{j=0}^{N-1}\left(|\phi_j^n|^2 + |\phi_{j+1}^n|^2\right) + k\tau\mathrm{Re}\sum_{l=1}^{n}\left(\phi_N^{l-\frac{1}{2}}\bar{\phi}_{N-1}^{l-\frac{1}{2}} - \phi_1^{l-\frac{1}{2}}\bar{\phi}_0^{l-\frac{1}{2}}\right), \quad n \geqslant 0, \tag{2.36}$$

$$\begin{aligned} E_2^n := {} & \frac{h}{4}\sum_{j=0}^{N-1}\left[2|\delta_x^+\phi_j^n|^2 + \beta(|\phi_j^n|^4 + |\phi_{j+1}^n|^4)\right] - kh\mathrm{Im}\sum_{j=1}^{N-1}\phi_j^n\delta_x\bar{\phi}_j^n \\ & + \frac{k\tau}{2}\mathrm{Im}\sum_{l=1}^{n}\left[\phi_{N-1}^{l-\frac{1}{2}}\delta_t^+\bar{\phi}_N^{l-1} + \phi_N^{l-\frac{1}{2}}\delta_t^+\bar{\phi}_{N-1}^{l-1} - \phi_0^{l-\frac{1}{2}}\delta_t^+\bar{\phi}_1^{l-1} - \phi_1^{l-\frac{1}{2}}\delta_t^+\bar{\phi}_0^{l-1}\right], \end{aligned} \tag{2.37}$$

respectively, where $Re(f)$ is the real part of function f and $\phi_j^{l+1/2} = \frac{1}{2}(\phi_j^{l+1} + \phi_j^l)$. Then similar to the proof of Lemma 2.2, for the TSFD-T method (2.34), we can prove that the mass is conserved in the discrete level, and respectively, for CNFD-T method (2.28)–(2.30), both the mass and energy are conserved in the discrete level:

Lemma 2.4. *The TSFD-T method (2.34) conserves the mass in the discrete level, and respectively, the CNFD-T method (2.28)–(2.30), conserves the mass and energy in the discrete level, i.e.*

$$N_2^n \equiv N_2^0, \quad E_2^n \equiv E_2^0, \quad n \geqslant 0. \tag{2.38}$$

It is easy to see that CNFD-T, SIFD-T and TSFD-T methods are implicit, time symmetric, second order in both space and time, and the memory cost is $O(N)$. The CNFD-T method is unconditionally stable and it conserves the mass and energy in the discrete level, however, it needs to solve a fully nonlinear coupled system at every time step which might be tedious in programming and time consuming in practical computation. The TSFD-T method is unconditionally stable and conserves the mass in the discrete level. The SIFD-T method is conditionally stable under the stability condition $\tau \leqslant 1/(|\beta| \max_{0\leqslant j\leqslant N, n\geqslant 0} |\psi_j^n|^2)$. Both TSFD-T and SIFD-T need only to solve a linear coupled system which can be solved very efficiently via Thomas algorithm, thus they are efficient and easy to program and the computational cost per time step is $O(N)$.

2.3. Numerical comparison of different methods

In this subsection, we compare numerically the accuracy of the above five numerical methods, i.e. CNFD, SIFD, CNFD-T, SIFD-T and TSFD-T, for simulating NLSE (1.1) when its solution has non-rest (or highly oscillatory) phase background at far field, e.g. type II dark soliton. To this end, we take $\beta = 1$ in (1.1) and the initial data ψ_0 in (1.12) as

$$\psi_0(x) = [a \tanh(a(x - x_0)) + i(v - k)] e^{i(kx+\theta_0)}, \quad x \in \mathbb{R},$$

with $a = 3, v = 2, k = 2$ and $x_0 = \theta_0 = 0$. Then the NLSE (1.1) with (1.12) has the exact type II dark soliton solution (1.11), i.e. $\psi(x,t) = \psi_{D2}(x,t)$ with the corresponding parameter values. In our computation, we take $L_1 = -4$ and $L_2 = 12$ which are large enough so that the truncation errors can be ignored. In order to quantify the numerical solution, we use the l^∞-norm of the error between the numerical solution ψ_j^n and the exact solution $\psi(x_j, t_n)$ as

$$e_\infty(t_n) := \max_{0\leqslant j\leqslant N} |\psi(x_j, t_n) - \psi_j^n|, \quad n \geqslant 0. \tag{2.39}$$

Table 2.1 shows the spatial and temporal errors $e_\infty(T = 2)$, i.e. at time $t_n = T = 2$, for the above five numerical methods under different mesh size h and time step τ.

From Table 2.1 and additional numerical results not shown here for brevity, we can draw the following conclusions: (i) all the five numerical methods are second-order accurate in both space and time, and thus they are comparable for solving

Table 2.1
Spatial and temporal error analysis of different numerical methods for NLSE (1.1) with highly oscillatory phase background at far field: (i) top half is for spatial error analysis with a very small time step $\tau = 10^{-5}$ under different mesh size h; (ii) bottom half is for temporal error analysis with a very small mesh size $h = 0.002$ under different time step τ.

h	$h_0 = 0.1$	$h_0/2$	$h_0/4$	$h_0/8$	$h_0/16$
CNFD	3.52E−1	8.74E−2	2.17E−2	5.42E−3	1.35E−3
SIFD	3.52E−1	8.74E−2	2.17E−2	5.42E−3	1.35E−3
CNFD-T	8.12E−2	1.96E−2	4.88E−3	1.22E−3	3.04E−4
SIFD-T	8.12E−2	1.96E−2	4.88E−3	1.22E−3	3.04E−4
TSFD-T	8.12E−2	1.96E−2	4.88E−3	1.22E−3	3.04E−4
τ	$\tau_0 = 0.025$	$\tau_0/2$	$\tau_0/4$	$\tau_0/8$	$\tau_0/16$
CNFD	2.64E−1	6.66E−2	1.66E−2	4.17E−3	1.05E−3
SIFD	5.07E−1	2.29E−1	5.33E−2	8.30E−3	1.63E−3
CNFD-T	2.64E−1	6.60E−2	1.65E−2	4.15E−3	1.06E−3
SIFD-T	5.07E−1	2.29E−1	5.32E−2	8.28E−3	1.58E−3
TSFD-T	1.44E−1	1.03E−2	2.58E−3	6.65E−4	1.68E−4

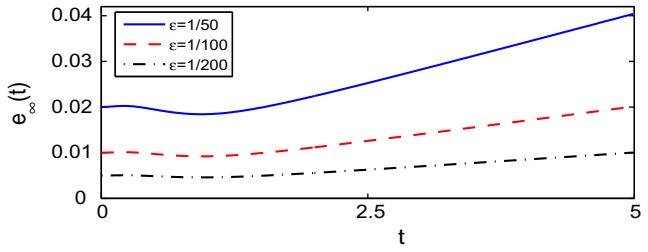

Fig. 2.1. Time evolution of the error $e_\infty(t) := \max_{L_1\leqslant x\leqslant L_2} |\psi(x,t) - \psi_{D2}(x,t)|$ between a type II dark soliton and its perturbation at different ε.

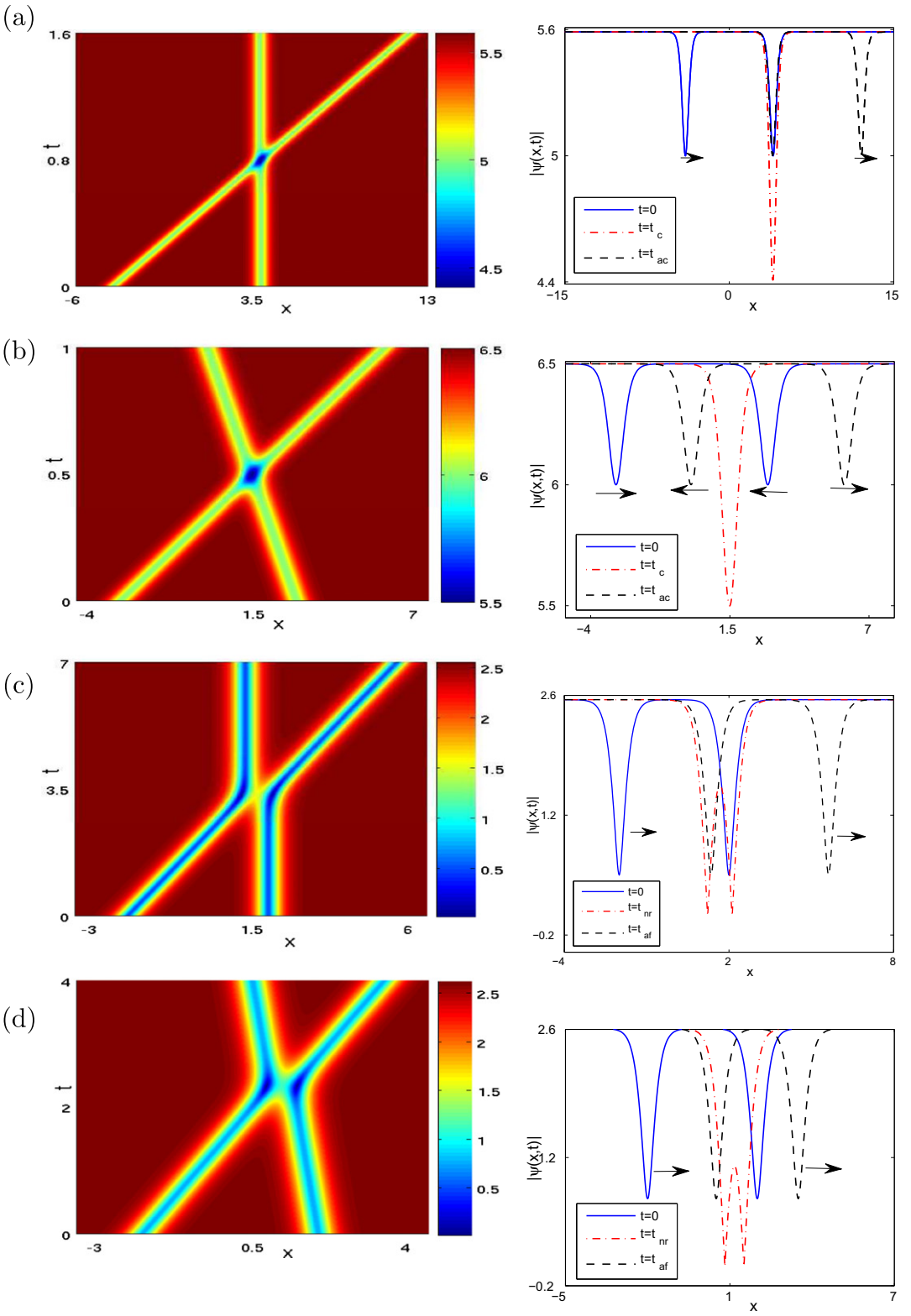

Fig. 2.2. Dynamics of the density $|\psi|$ for the interaction of two type II dark solitons of NLSE (1.1) with $a = 2.5$ and different parameter values: (i) 'fast' motion of phase background under $k = 5$, $v_2 = 0$, $v_1 = 2k = 10$ and $x_0 = 4$ (a); and $k = 3$, $v_1 = 3k = 9$, $v_2 = -k = -3$ and $x_0 = 3$ (b); and (ii) 'slow' motion of phase background with $k = 0.5$ under $v_2 = 0$, $v_1 = 2k = 1$ and $x_0 = 2$ (c); and $v_1 = 2.5k = 1.25$, $v_2 = -0.5k = -0.25$ and $x_0 = 2$ (d).

NLSE. (ii) In general, for fixed mesh size h, CNFD and SIFD have the same spatial discretization error, and CNFD-T, SIFD-T and TSFD-T have the same spatial discretization error which is much smaller than that of CNFD and SIFD. (iii) In general, for fixed time step τ, SIFD and SIFD-T have the same temporal discretization error, CNFD and CNFD-T have the same temporal discretization error which is about half of SIFD and SIFD-T methods, TSFD-T has the smallest temporal discretization error among the five numerical methods. (iv) Based on the above comparison, we suggest that TSFD-T is the best numerical method among the five numerical methods since it is the most accurate, unconditional stable, easy to program, less computational cost per time step; and it conserves the mass in the discrete level.

2.4. Stability and interaction of type II dark solitons

Now we apply the TSFD-T method to study numerically the stability of type II dark soliton and their interactions of NLSE (1.1). To this end, we take $\beta = 1$ in (1.1). For the study of stability, we choose the initial data ψ_0 in (1.12) as a type II dark soliton with a perturbation as

$$\psi_0(x) = [a\tanh(a(x-x_0)) + i(v-k)]e^{i(kx+\theta_0)} + \varepsilon e^{-(x-x_0+x_1)^2}, \quad x \in \mathbb{R},$$

with $a = 1, v = 1, k = 1, x_1 = 0.1, x_0 = -2.5$ and $\theta_0 = 0$. The problem is solved numerically on $\Omega = [L_1, L_2]$ with $L_1 = -15$ and $L_2 = 15$, mesh size $h = 0.006$ and time step $\tau = 10^{-3}$. Fig. 2.1 depicts the time evolution of the error between the solution ψ of the NLSE (1.1) with the above initial data and its corresponding type II dark soliton ψ_{D2} in (1.11) with the corresponding parameter values, i.e. $e(t) := \max_{L_1 \leqslant x \leqslant L_2} |\psi(x,t) - \psi_{D2}(x,t)|$, under different ε. This result clearly demonstrates that the type II dark soliton (1.11) is dynamically stable in the NLSE (1.1). Similarly, for the study of the interaction between two type II dark solitons, we choose the initial data ψ_0 in (1.12) as

$$\psi_0(x) = e^{ikx}\begin{cases} [a\tanh(a(x+x_0)) + i(v_1-k)], & -\infty < x < 0, \\ -[a\tanh(a(x-x_0)) + i(v_2-k)], & 0 \leqslant x < \infty, \end{cases} \tag{2.40}$$

where $x_0 > 0$ is chosen such that the two dark solitons are initially centered at $x = \pm x_0$ and well-separated, $k \neq 0$ is the 'velocity' of the phase background, $v_1 \geqslant 0$ and $v_2 \leqslant 0$ satisfying $v_1 + v_2 = 2k$ are the velocities of the left-going soliton and right-going soliton, respectively. The problem is solved numerically on $\Omega = [L_1, L_2]$ with $L_1 = -15$ and $L_2 = 15$, mesh size $h = 0.02$ and time step $\tau = 10^{-4}$.

Before presenting the numerical result, we define the following four times which will be used hereafter. In the case when the two solitons can be transmitted through each other, we denote t_c as the time when the two soliton completely collide (or overlap) with each other and $t_{ac} (> t_c)$ as some time after collision, i.e. the time when two soliton go across each other and completely separated again. In the case when the two solitons cannot go across each other, we denote t_{nr} as the time when the two soliton come closest to each other, and $t_{af} (> t_{nr})$ as some time afterward when the two soliton separate again.

Fig. 2.2 shows time evolution of the density $|\psi|$ for the interaction of two type II dark solitons of NLSE under different parameter values of x_0, k, a, v_1 and v_2.

From Fig. 2.2 and additional numerical results not shown here for brevity, we can draw the following conclusions for the interaction of two type II dark solitons of NLSE: (i) The interaction of two initially well-separated type II dark solitons is repulsive. If the velocity of the two solitons are both small enough, they cannot be transmitted through each other. Otherwise, they will pass through each other without any oscillation created. (ii) At the collision, the peak value of the amplitude is equal to the sum of the peak values of the two solitons initially. (iii) After collision, the two solitons separate completely and recover their initial velocities and profiles which again demonstrates the NLSE (1.1) is an integrable system even for the interaction of type II dark solitons.

3. Numerical methods for NLSE with type I dark solitons

In this section, we will compare different numerical methods for the NLSE (1.1) with (1.12) when the solution admits type I dark soliton at far field, i.e. the solution has nonzero but rest background at far field. We assume that the initial data ψ_0 satisfies

$$\psi_0(x) \to A_\pm^0, \quad x \to \pm\infty, \tag{3.1}$$

where $A_+ \neq A_-$ are two given complex constants. Similar to those in Section 2, we have

$$\psi(x,t) \to A_\pm^0 e^{-i(k^2 + 2\beta|A_\pm^0|^2)t/2}, \quad x \to \pm\infty, \quad t \geqslant 0. \tag{3.2}$$

This implies that the solution $\psi(x,t)$ of the NLSE (1.1) with (1.12) has nonzero time-dependent rest background at far field.

3.1. Numerical methods

Based on the far field asymptotic behavior (3.2) of the solution ψ, differentiating (3.2) with respect to x, we get

$$\partial_x \psi(x,t) \to 0, \quad x \to \pm\infty, \quad t \geqslant 0. \tag{3.3}$$

Thus the original problem (1.1) with (1.12) can be truncated and approximated as

$$i\partial_t\psi(x,t) = -\frac{1}{2}\partial_{xx}\psi(x,t) + \beta|\psi(x,t)|^2\psi(x,t), \quad L_1 < x < L_2, \quad t > 0, \tag{3.4}$$

$$\partial_x\psi(L_1,t) = \partial_x\psi(L_2,t) = 0, \quad t > 0, \tag{3.5}$$

$$\psi(x,0) = \psi_0(x), \quad L_1 \leqslant x \leqslant L_2. \tag{3.6}$$

For the above problem, we can define the *mass* and *energy* as

$$N_3(t) := \int_{L_1}^{L_2} |\psi(x,t)|^2 dx, \quad E_3(t) := \frac{1}{2}\int_{L_1}^{L_2} (|\partial_x\psi|^2 + \beta|\psi|^4) dx, \quad t \geqslant 0. \tag{3.7}$$

Then similar to the proof of Lemma 2.1, we can prove that the mass and energy are conserved:

Lemma 3.1. *The truncated problem (3.4)–(3.6) conserves the mass and energy (3.7), i.e.*

$$N_3(t) \equiv N_3(0) = \int_{L_1}^{L_2} |\psi_0(x)|^2 dx, \quad E_3(t) \equiv E_3(0) = \frac{1}{2}\int_{L_1}^{L_2} (|\partial_x\psi_0|^2 + \beta|\psi_0|^4) dx, \quad t \geqslant 0. \tag{3.8}$$

For the numerical discretization of (3.4)–(3.6), the CNFD method (2.12)–(2.14) and SIFD method (2.15) with (2.13) and (2.14) are still valid provided that we set $k = 0$ in them; and the TSFD method (2.34) is still valid provided that we set $k = 0$ and replace ϕ by ψ in it. In addition, we can also discretize (2.33) with $k = 0$ and ϕ replaced by ψ, which can be viewed as a free Schrödinger equation from (3.4) by applying the time-splitting technique, via a cosine pseudospectral method [36]. In fact, denote the grid points as $x_{j+\frac{1}{2}} := L_1 + h(j+\frac{1}{2})$ for $j = 0, 1, \ldots, N-1$, and $\mu_l = \frac{l\pi}{L_2 - L_1}$ for $l = 0, 1, \ldots, N-1$, let $\psi^n_{j+\frac{1}{2}}$ be the numerical approximation of $\psi(x_{j+\frac{1}{2}}, t_n)$ for $j = 0, 1, \ldots, N-1$ and $n \geqslant 0$. Then a time-splitting cosine pseudospectral (TSCP) method for discretizing the problem (3.4)–(3.6) reads as [8]

$$\psi^{(1)}_{j+\frac{1}{2}} = e^{-i\beta\tau|\psi^n_{j+\frac{1}{2}}|^2/2}\psi^n_{j+\frac{1}{2}},$$

$$\psi^{(2)}_{j+\frac{1}{2}} = \sum_{l=0}^{N-1} \alpha_l e^{-i\mu_l^2\tau/2}\widehat{\psi^{(1)}_l}\cos(\mu_l(x_{j+\frac{1}{2}} - L_1)),$$

$$\psi^{n+1}_{j+\frac{1}{2}} = e^{-i\beta\tau|\psi^{(2)}_{j+\frac{1}{2}}|^2/2}\psi^{(2)}_{j+\frac{1}{2}}, \quad j = 0, 1, \ldots, N-1, \quad n \geqslant 0, \tag{3.9}$$

where $\widehat{\psi^{(1)}_l}$ $(l = 0, 1, \ldots, N-1)$ are the discrete cosine transform coefficients defined as

$$\widehat{\psi^{(1)}_l} = \alpha_l \sum_{j=0}^{N-1} \psi^{(1)}_{j+\frac{1}{2}} \cos(\mu_l(x_{j+\frac{1}{2}} - L_1)), \quad l = 0, 1, \ldots, N-1.$$

with

$$\alpha_0 = \sqrt{\frac{1}{N}}, \quad \alpha_l = \sqrt{\frac{2}{N}}, \quad 1 \leqslant l \leqslant N-1.$$

Similar to those in Section 2.2, we can prove that CNFD, TSFD and TSCP methods conserve the mass in the discrete level, meanwhile CNFD method also conserves the energy in the discrete level. Moreover, CNFD, SIFD, TSFD and TSCP are time symmetric and the memory cost is $O(N)$. Furthermore, CNFD, SIFD and TSFD methods are implicit and second order in both space and time, while TSCP is explicit, second order in time and spectral order in space. In addition, CNFD, TSFD and TSCP are unconditionally stable, while SIFD method is conditionally stable under the stability condition $\tau \leqslant 1/(|\beta|\max_{0\leqslant j\leqslant N, n\geqslant 0}|\psi^n_j|^2)$. At every time step, CNFD method needs to solve a fully nonlinear coupled system which might be tedious in programming and time consuming in practical computation, and both SIFD and TSFD methods need only to solve a linear coupled system which can be solve very efficiently via Thomas algorithm, thus they are efficient and easy to program and the computational cost per time step is $O(N)$. The computational cost of TSCP per time step is $O(N\ln N)$ via the discrete cosine transform (DCT).

3.2. Numerical comparison of different methods

In this subsection, we compare numerically the accuracy of the above four numerical methods, i.e. CNFD, SIFD, TSFD and TSCP, for simulating NLSE (1.1) when its solution has nonzero rest background at far field, e.g. type I dark solitons. To this end, we take $\beta = 1$ in (1.1) and the initial data ψ_0 in (1.12) as

$$\psi_0(x) = [iv + a\tanh(a(x - x_0))]e^{i\theta_0}, \quad x \in \mathbb{R},$$

with $a = 2$, $v = 1$ and $x_0 = \theta_0 = 0$. Then the NLSE (1.1) with (1.12) has the exact type I dark soliton solution (1.10), i.e. $\psi(x,t) = \psi_{D1}(x,t)$ with the corresponding parameter values. In our computation, we take $L_1 = -15$ and $L_2 = 30$ which are large enough so that the truncation errors can be ignored. Table 3.1 shows the spatial and temporal errors $e_\infty(T = 2)$ defined in (2.39) for the above four numerical methods under different mesh size h and time step τ.

From Table 3.1 and additional numerical results not shown here for brevity, we can draw the following conclusions: (i) CNFD, SIFD and TSFD methods are second-order accurate in both space and time, while TSCP is second-order accurate in time and spectral accurate in space. (ii) In general, for fixed mesh size h, CNFD, SIFD and TSFD have the same spatial discretization error, and TSCP has much smaller spatial discretization error. (iii) In general, for fixed time step τ, SIFD and CNFD have similar temporal discretization error, TSFD and TSCP have similar temporal discretization error which is usually about one order of magnitude smaller than that of SIFD and CNFD when τ is small. (iv) Based on the above comparison, in general, we suggest that TSCP is the best one among the four numerical methods since it is the most accurate, unconditional stable, easy to program, and it conserves the mass in the discrete level.

3.3. Stability and interaction of type I dark solitons

Now we apply the TSCP method to study numerically the stability of type I dark soliton and their interactions of NLSE (1.1). To this end, we take $\beta = 1$ in (1.1). For the study of stability, we choose the initial data ψ_0 in (1.12) as a type I dark soliton with a perturbation as

$$\psi_0(x) = [iv + a\tanh(a(x - x_0))]e^{i\theta_0} + \varepsilon e^{-(x-x_0+x_1)^2}, \quad x \in \mathbb{R},$$

with $a = 2$, $v = 2, x_1 = 0.1, x_0 = 5$ and $\theta_0 = 0$. The problem is solved numerically on $\Omega = [L_1, L_2]$ with $L_1 = -25$ and $L_2 = 25$, mesh size $h = 0.05$ and time step $\tau = 10^{-4}$. Fig. 3.1 depicts the time evolution of the error between the solution ψ of the NLSE (1.1) with the above initial data and its corresponding type I dark soliton ψ_{D1} in (1.10) with the corresponding parameter values, i.e. $e(t) := \max_{L_1 \leqslant x \leqslant L_2} |\psi(x,t) - \psi_{D1}(x,t)|$, under different ε. This result clearly demonstrates that the type I dark soliton (1.10) is dynamically stable in the NLSE (1.1). Similarly, for the study of interaction between two type I dark solitons, we choose the initial data ψ_0 in (1.12) as

$$\psi_0(x) = \begin{cases} iv + a\tanh(a(x + x_0)), & -\infty < x < 0, \\ -[-iv + a\tanh(a(x - x_0))], & 0 \leqslant x < \infty, \end{cases} \tag{3.10}$$

where $x_0 > 0$ is chosen such that the two type I dark solitons are initially centered at $x = \pm x_0$ and well-separated, $v > 0$ is the velocity of the soliton centered at $x = -x_0$ at $t = 0, a > 0$ is a constant. The problem is solved numerically on $\Omega = [L_1, L_2]$ with

Table 3.1
Spatial and temporal error analysis of different numerical methods for NLSE (1.1) with nonzero rest background at far field: (i) top half is for spatial error analysis with a very small time step $\tau = 10^{-6}$ under different mesh size h; (ii) bottom half is for temporal error analysis with a very small mesh size $h = 0.005$ under different time step τ.

h	h_0 = 0.45	$h_0/2$	$h_0/4$	$h_0/8$	$h_0/16$
CNFD	4.65E−1	1.13E−1	2.68E−2	6.63E−3	1.66E−3
SIFD	4.65E−1	1.13E−1	2.68E−2	6.63E−3	1.66E−3
TSFD	4.65E−1	1.13E−1	2.68E−2	6.63E−3	1.66E−3
TSCP	2.85E−2	2.76E−5	1.06E−9	<1E−9	<1E−9
τ	τ_0=0.05	$\tau_0/2$	$\tau_0/4$	$\tau_0/8$	$\tau_0/16$
CNFD	1.33E−1	3.35E−2	8.42E−3	2.13E−3	5.52E−4
SIFD	3.73E−1	9.78E−2	2.26E−2	4.72E−3	1.08E−3
TSFD	1.28E−2	3.20E−3	8.32E−4	2.10E−4	5.28E−5
TSCP	5.50E−1	1.21E−2	8.34E−4	2.12E−4	5.30E−5

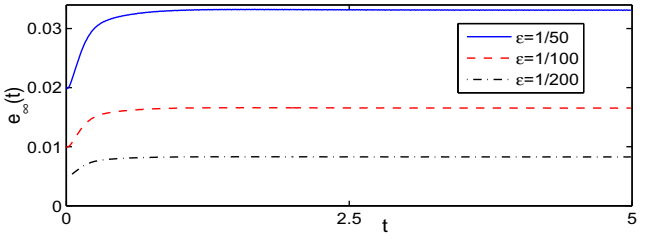

Fig. 3.1. Time evolution of the error $e_\infty(t) := \max_{L_1 \leqslant x \leqslant L_2} |\psi(x,t) - \psi_{D1}(x,t)|$ between a type I dark soliton and its perturbation at different ε.

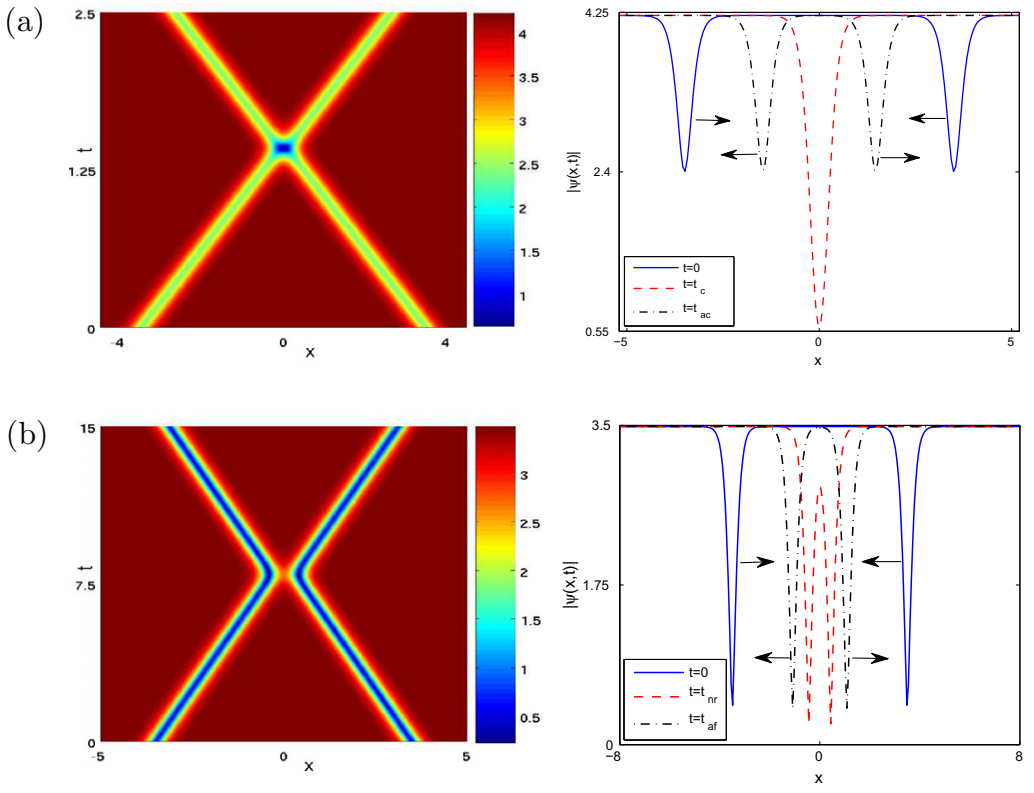

Fig. 3.2. Dynamics of the density $|\psi|$ for the interaction of two type I dark solitons of NLSE (1.1) with $x_0 = 3.5$ and $a = 2\sqrt{3}$ under different velocities: (a) 'high' velocity $v = \frac{1.2a}{\sqrt{3}}$; and (b) 'low' velocity $v = \frac{0.2a}{\sqrt{3}}$.

$L_1 = -15$ and $L_2 = 15$, mesh size $h = 0.03$ and time step $\tau = 10^{-3}$. Fig. 3.2 displays time evolution of the density $|\psi|$ for the interaction of two type I dark solitons of NLSE under different parameter values of x_0, a and v.

From Fig. 3.2 and additional numerical results not shown here for brevity, we can draw the following conclusions for the interaction of two type I dark solitions in NLSE: (i) The interaction of two initially well-separated type I dark solitons is repulsive. After the interaction, the two solitons separate completely. (ii) Before the two solitons meet each other or after they separate completely, the two solitons move at constant velocities and preserves their profiles in density exactly. During the interaction, there is no oscillation occurs. (iii) For fixed amplitude $a > 0$, there exists a critical $v_c(a) > 0$ depending only on the amplitude a. When $0 < v < v_c(a)$, the two solitons cannot go across each other, they slow down when they move towards each other, then stop moving before meeting each other, and finally reflect and move away from each other. On the contrary, when $v > v_c(a)$, the two solitons move across each other without changing their direction, they come close to each other and collide, then across with each other and continue their motion without changing their velocities. (iv) By our extensive numerical results, we find numerically the critical velocity $v_c(a)$ satisfies

$$v_c(a) = 0.5455a + 0.0505, \quad a > 0.$$

In addition, if collision happens, then the peak value of the amplitude at the collision is equal to the sum of the peak values of the two solitons initially.

4. Numerical methods for NLSE with bright solitons

In this section, we will compare different numerical methods for the NLSE (1.1) with (1.12) when the solution admits bright soliton at far field, i.e. the solution decays to zero at far field. We assume that the initial data ψ_0 satisfies

$$\psi_0(x) \to 0, \quad x \to \pm\infty. \tag{4.1}$$

Similar to those in Section 2, we have

$$\psi(x,t) \to 0, \quad x \to \pm\infty, \quad t \geqslant 0. \tag{4.2}$$

This implies that the solution $\psi(x,t)$ of the NLSE (1.1) with (1.12) decays to zero at far field.

4.1. Numerical methods

Based on the far field asymptotic behavior (4.2) of the solution ψ, the original problem (1.1) with (1.12) can be truncated and approximated as

$$i\partial_t\psi(x,t) = -\frac{1}{2}\partial_{xx}\psi(x,t) + \beta|\psi(x,t)|^2\psi(x,t), \quad L_1 < x < L_2, \quad t > 0, \tag{4.3}$$

$$\psi(x,0) = \psi_0(x), \quad L_1 \leqslant x \leqslant L_2, \tag{4.4}$$

with either the homogeneous Neumann boundary condition

$$\partial_x\psi(L_1,t) = \partial_x\psi(L_2,t) = 0, \quad t > 0, \tag{4.5}$$

or the homogeneous Dirichlet boundary condition

$$\psi(L_1,t) = \psi(L_2,t) = 0, \quad t > 0, \tag{4.6}$$

or the periodic boundary condition

$$\psi(L_1,t) = \psi(L_2,t), \quad \partial_x\psi(L_1,t) = \partial_x\psi(L_2,t), \quad t > 0. \tag{4.7}$$

Again, similar to the proof of Lemma 2.1, we can prove that the above problem (4.3)–(4.4) with either (4.5) or (4.6) or (4.7) conserves the mass and energy defined in (3.7).

For the numerical discretization, when the homogeneous Neumann boundary condition (4.5) is used, i.e. (4.3)–(4.5), all the four numerical methods CNFD, SIFD, TSFD and TSCP we have discussed in Section 3 can be applied straightforward. When the homogeneous Dirichlet boundary condition (4.6) is used, i.e. (4.3)–(4.4) with (4.6), the CNFD (2.12), SIFD (2.15) and TSFD (2.34) methods are still valid provided that we replace $0 \leqslant j \leqslant N$ by $1 \leqslant j \leqslant N-1$, and set $k = 0$ and replace ϕ by ψ in (2.34), meanwhile we replace the boundary discretization in (2.13) and (2.35) by

$$\psi_0^{n+1} = \psi_N^{n+1} = 0, \quad \text{and} \quad \psi_0^{(2)} = \psi_N^{(2)} = 0 \quad n \geqslant 0,$$

respectively. In addition, we can also discretize (2.33) with $k = 0$ and ϕ replaced by ψ, which can be viewed as a free Schrödinger equation from (4.3) with homogeneous Dirichlet boundary condition by applying the time-splitting technique, via a sine pseudospectral method [36]. In fact, a time-splitting sine pseudospectral (TSSP) method for discretizing the problem (4.3)–(4.4) with (4.6) reads as [13]

$$\psi_j^{(1)} = e^{-i\beta\tau|\psi_j^n|^2/2}\psi_j^n,$$

$$\psi_j^{(2)} = \sum_{l=0}^{N-1} e^{-i\mu_l^2\tau/2}\widehat{\psi_l^{(1)}}\sin(\mu_l(x_j - L_1)),$$

$$\psi_j^{n+1} = e^{-i\beta\tau|\psi_j^{(2)}|^2/2}\psi_j^{(2)}, \quad j = 1,2,\ldots,N-1, \quad n \geqslant 0, \tag{4.8}$$

where $\widehat{\psi_l^{(1)}}$ $(l = 1,2,\ldots,N-1)$ are the discrete sine transform coefficients defined as

$$\widehat{\psi_l^{(1)}} = \frac{2}{N}\sum_{j=1}^{N-1}\psi_j^{(1)}\sin(\mu_l(x_j - L_1)), \quad l = 1,2,\ldots,N-1.$$

Similarly, when the periodic boundary condition (4.7) is used, i.e. (4.3)–(4.4) with (4.7), again, the CNFD (2.12), SIFD (2.15) and TSFD (2.34) methods are still valid provided that we replace $0 \leqslant j \leqslant N$ by $0 \leqslant j \leqslant N-1$, and set $k = 0$ and replace ϕ by ψ in (2.34); and the boundary discretization in (2.13) and (2.35) replaced by

$$\psi_{-1}^{n+1} = \psi_{N-1}^{n+1}, \quad \psi_N^{n+1} = \psi_0^{n+1}, \quad \text{and} \quad \psi_{-1}^{(2)} = \psi_{N-1}^{(2)}, \quad \psi_N^{(2)} = \psi_0^{(2)}, \quad n \geqslant 0,$$

respectively. In addition, we can also discretize (2.33) with $k = 0$ and ϕ replaced by ψ, which can be viewed as a free Schrödinger equation from (4.3) with periodic boundary condition by applying the time-splitting technique, via a Fourier pseudospectral method [36]. In fact, a time-splitting Fourier pseudospectral (TSFP) method for discretizing the problem (4.3)–(4.4) with (4.7) reads as [10]

$$\psi_j^{(1)} = e^{-i\beta\tau|\psi_j^n|^2/2}\psi_j^n,$$

$$\psi_j^{(2)} = \sum_{l=-N/2}^{N/2-1} e^{-i\lambda_l^2\tau/2}\widehat{\psi_l^{(1)}}e^{i\lambda_l(x_j - L_1)},$$

$$\psi_j^{n+1} = e^{-i\beta\tau|\psi_j^{(2)}|^2/2}\psi_j^{(2)}, \quad j = 0, 1, \ldots, N-1, \quad n \geqslant 0, \tag{4.9}$$

where $\lambda_l = \frac{2l\pi}{L_2 - L_1}$ for $l = -N/2, \ldots, N/2-1$ and $\widehat{\psi_l^{(1)}}$ $(l = -N/2, \ldots, N/2-1)$ are the discrete Fourier transform coefficients defined as

$$\widehat{\psi_l^{(1)}} = \frac{1}{N}\sum_{j=0}^{N-1}\psi_j^{(1)} e^{-i\lambda_l(x_j - L_1)}, \quad l = -\frac{N}{2}, \ldots, \frac{N}{2}-1.$$

Again, similar to those in Section 2.2, we can prove that CNFD, TSFD, TSCP TSSP and TSFP methods conserve the mass in the discrete level, meanwhile CNFD method also conserves the energy in the discrete level. Moreover, CNFD, SIFD, TSFD, TSCP, TSSP and TSFP methods are time symmetric and the memory cost is $O(N)$. Furthermore, CNFD, SIFD and TSFD methods are implicit and second order accurate in both space and time, while TSCP, TSSP and TSFP methods are explicit, and second order in time and spectral order in space. In addition, CNFD, TSFD, TSSP, TSFP and TSCP methods are unconditionally stable, while SIFD method is conditionally stable under the stability condition $\tau \leqslant 1/(|\beta|\max_{0\leqslant j\leqslant N, n\geqslant 0}|\psi_j^n|^2)$. At every time step, CNFD method needs to solve a fully nonlinear coupled system which might be tedious in programming and time consuming in practical computation, and both SIFD and TSFD methods need only to solve a linear coupled system which can be solved very efficiently via Thomas algorithm, thus they are efficient and easy to program and the computational cost per time step is $O(N)$. The computational cost of TSCP, TSSP and TSFP per time step is $O(N\ln N)$ via DCT, discrete sine transform (DST) and fast Fourier transform (FFT).

4.2. Numerical comparison of different methods

In this subsection, we compare numerically the accuracy of the above six numerical methods, i.e. CNFD, SIFD, TSFD, TSCP, TSSP and TSFP for simulating NLSE (1.1) when its solution decays to zero at far field, e.g. bright solitons. To this end, we take $\beta = -1$ in (1.1) and the initial data ψ_0 in (1.12) as

$$\psi_0(x) = a\,\mathrm{sech}(a(x - x_0))e^{i(vx+\theta_0)}, \quad x \in \mathbb{R},$$

with $a = 2, v = 1$ and $x_0 = \theta_0 = 0$. Then the NLSE (1.1) with (1.12) has the exact bright soliton solution (1.5), i.e. $\psi(x,t) = \psi_B(x,t)$ with the corresponding parameter values. In our computation, we take $L_1 = -15$ and $L_2 = 20$ which are large enough so that the truncation errors can be ignored. Table 4.1 shows the spatial and temporal errors $e_\infty(T = 5)$ defined in (2.39) for the above numerical methods under different mesh size h and time step τ when the original problem is truncated via the homogeneous Neumann boundary condition (4.5), Tables 4.2 and 4.3 depict similar results when the homogeneous Dirichlet boundary condition (4.6) and periodic boundary condition (4.7) are applied, respectively.

From Tables 4.1,4.2,4.3 and additional numerical results not shown here for brevity, we can draw the following conclusions: (i) CNFD, SIFD and TSFD methods are second-order accurate in space and time, while TSCP, TSSP and TSFP methods are second-order accurate in time and spectral accurate in space. (ii) In general, for fixed mesh size h, CNFD, SIFD and TSFD methods have the same spatial discretization error, and TSCP, TSSP and TSFP methods have the same spatial discretization error which is much smaller than that of CNFD, SIFD and TSFD methods. (iii) In general, for fixed time step τ, TSFD, TSCP, TSSP and TSFP methods have similar temporal discretization error, SIFD and CNFD methods have the largest and smallest errors in temporal discretization, respectively, they are all in the same order of magnitude. (iv) Based on the above comparison, in general, we suggest that either TSSP or TSCP or TSFP can be used among the above numerical methods since they are the most accurate, unconditional stable, easy to program; and they conserve the mass in the discrete level.

Table 4.1
Spatial and temporal error analysis of different numerical methods for NLSE (1.1) with zero far field condition when the homogeneous Neumann boundary condition (4.5) is used in the truncation: (i) top half is for spatial error analysis with a very small time step $\tau = 10^{-5}$ under different mesh size h; (ii) bottom half is for temporal error analysis with a very small mesh size $h = 0.0035$ under different time step τ.

h	$h_0 = 0.5$	$h_0/2$	$h_0/4$	$h_0/8$	$h_0/16$
CNFD	2.48	8.50E−1	1.79E−1	4.33E−2	1.07E−2
SIFD	2.48	8.50E−1	1.79E−1	4.33E−2	1.07E−2
TSFD	2.48	8.50E−1	1.79E−1	4.33E−2	1.07E−2
TSCP	3.15E−1	2.44E−4	4.35E−9	<1E−9	<1E−9
τ	$\tau_0 = 0.1$	$\tau_0/2$	$\tau_0/4$	$\tau_0/8$	$\tau_0/16$
CNFD	1.07E−1	2.71E−2	6.72E−3	1.58E−3	2.95E−4
SIFD	7.61E−1	1.23E−1	2.91E−2	7.23E−3	1.85E−3
TSFD	3.74E−1	8.52E−2	2.10E−2	5.31E−3	1.38E−3
TSCP	2.18E−1	5.90E−2	1.51E−2	3.79E−3	9.50E−4

Table 4.2
Spatial and temporal error analysis of different numerical methods for NLSE (1.1) with zero far field condition when the homogeneous Dirichlet boundary condition (4.6) is used in the truncation: (i) top half is for spatial error analysis with a very small time step $\tau = 10^{-5}$ under different mesh size h; (ii) bottom half is for temporal error analysis with a very small mesh size $h = 0.0035$ under different time step τ.

h	$h_0 = 0.5$	$h_0/2$	$h_0/4$	$h_0/8$	$h_0/16$
CNFD	2.48	8.50E−1	1.79E−1	4.33E−2	1.07E−2
SIFD	2.48	8.50E−1	1.79E−1	4.33E−2	1.07E−2
TSFD	2.48	8.50E−1	1.79E−1	4.33E−2	1.07E−2
TSSP	3.95E−1	2.22E−4	3.93E−9	<1E−9	<1E−9
τ	$\tau_0 = 0.1$	$\tau_0/2$	$\tau_0/4$	$\tau_0/8$	$\tau_0/16$
CNFD	1.07E−1	2.71E−2	6.72E−3	1.58E−3	2.95E−4
SIFD	7.61E−1	1.23E−1	2.88E−2	7.19E−3	1.81E−3
TSFD	3.74E−1	8.52E−2	2.10E−2	5.31E−3	1.35E−3
TSSP	2.18E−1	5.90E−2	1.51E−2	3.79E−3	9.49E−4

Table 4.3
Spatial and temporal error analysis of different numerical methods for NLSE (1.1) with zero far field condition when the periodic boundary condition (4.7) is used in the truncation: (i) top half is for spatial error analysis with a very small time step $\tau = 10^{-5}$ under different mesh size h; (ii) bottom half is for temporal error analysis with a very small mesh size $h = 0.0035$ under different time step τ.

h	$h_0 = 0.5$	$h_0/2$	$h_0/4$	$h_0/8$	$h_0/16$
CNFD	2.48	8.50E−1	1.79E−1	4.33E−2	1.07E−2
SIFD	2.48	8.50E−1	1.79E−1	4.33E−2	1.07E−2
TSFD	2.48	8.50E−1	1.79E−1	4.33E−2	1.07E−2
TSFP	3.94E−1	2.21E−4	3.93E−9	<1E−9	<1E−9
τ	$\tau_0 = 0.1$	$\tau_0/2$	$\tau_0/4$	$\tau_0/8$	$\tau_0/16$
CNFD	1.07E−1	2.71E−2	6.72E−3	1.58E−3	2.95E−4
SIFD	7.61E−1	1.23E−1	2.91E−2	7.19E−3	1.79E−3
TSFD	3.74E−1	8.52E−2	2.10E−2	5.31E−3	1.37E−3
TSFP	2.18E−1	5.90E−2	1.53E−2	3.81E−3	9.50E−4

4.3. Stability and interaction of bright solitons

For completeness, here we also apply the TSCP method to study numerically the stability of bright soliton and their interactions of NLSE (1.1). To this end, we take $\beta = -1$ in (1.1). For the study of stability, we choose the initial data ψ_0 in (1.12) as a bright soliton with a perturbation as

$$\psi_0(x) = a\,\mathrm{sech}(a(x - x_0))e^{i(vx+\theta_0)} + \varepsilon e^{-(x-x_0+x_1)^2}, \quad x \in \mathbb{R},$$

with $a = 1$, $v = 1, x_1 = 0.1, x_0 = -5$ and $\theta_0 = 0$. The problem is solved numerically on $\Omega = [L_1, L_2]$ with $L_1 = -25$ and $L_2 = 25$, mesh size $h = 0.05$ and time step $\tau = 10^{-4}$. Fig. 4.1 displays the time evolution of the error between the solution ψ of the NLSE (1.1) with the above initial data and its corresponding bright soliton ψ_B in (1.5) with the corresponding parameter values, i.e. $e_\infty(t) := \max_{L_1 \leqslant x \leqslant L_2} |\psi(x,t) - \psi_B(x,t)|$, under different ε. This result clearly demonstrates that the bright soliton (1.5) is dynamically stable in the NLSE (1.1).

Similarly, for the study of interactions between two bright solitons, we choose the initial data ψ_0 in (1.12) as

$$\psi_0(x) = a_1\,\mathrm{sech}(a_1(x - x_0))e^{iv_1x} + a_2\,\mathrm{sech}(a_2(x + x_0))e^{iv_2x}, \quad x \in \mathbb{R}, \tag{4.10}$$

where $x_0 = 15 > 0$ is chosen such that the two bright solitons are initially centered at $x = \pm x_0$ and well-separated, $v_1 < 0$ and $v_2 > 0$ are the velocities of two solitons at $t = 0, a_1 > 0$ and $a_2 > 0$ are the amplitudes of the two solitons. The problem is

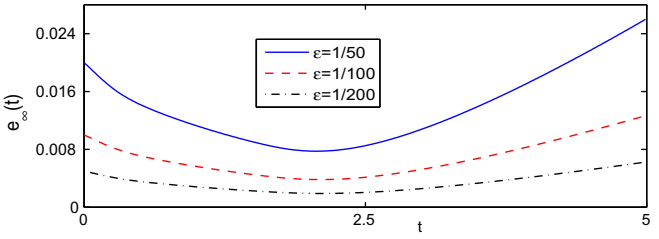

Fig. 4.1. Time evolution of the error $e_\infty(t) := \max_{L_1 \leqslant x \leqslant L_2} |\psi(x,t) - \psi_B(x,t)|$ between a bright soliton and its perturbation at different ε.

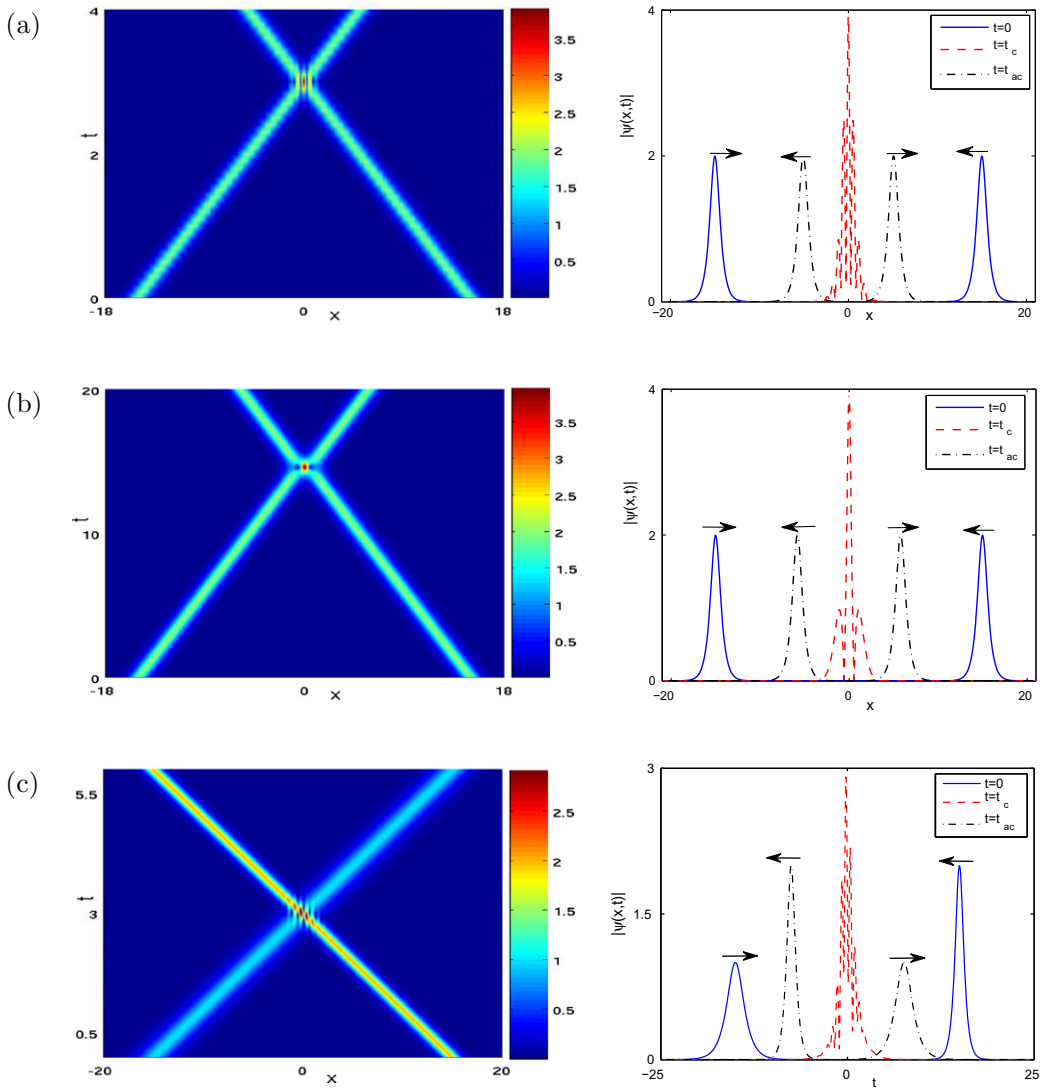

Fig. 4.2. Dynamics of the density $|\psi|$ for the interaction of two bright solitons of NLSE (1.1) with $x_0 = 15$ under different cases: (a) 'high' velocity $a_1 = a_2 = 2$, $v_1 = 5$ and $v_2 = -5$; (b) 'low' velocity $a_1 = a_2 = 2$, $v_1 = 1$ and $v_2 = -1$; and (c) different amplitudes with the same velocity $a_1 = 2$, $a_2 = 1$, $v_1 = 5$ and $v_2 = -5$.

solved numerically with $L_1 = -30$ and $L_2 = 30$, mesh size $h = 0.05$ and time step $\tau = 10^{-3}$. Fig. 4.2 shows time evolution of the density $|\psi|$ for the interaction of two bright solitons of NLSE under different parameter values of a_1, a_2, v_1 and v_2.

From Fig. 4.2 and additional numerical results not shown here for brevity, we can draw the following conclusions for the interaction of two bright solitons in NLSE: (i) The interaction of two initially well-separated bright solitons is attractive. After the interaction, the two solitons separate completely. (ii) Before the two solitons meet each other or after they separate completely, the two solitons move at constant velocities and preserves their profiles in density exactly. During the interaction, there is oscillation created. In general, the larger the velocity is, the stronger the oscillation will be. (iii) At the collision, the peak value of the amplitude is equal to the sum of the peak values of the two solitons initially.

5. Extension to NLSE with general nonlinearity and coupled NLSEs

The ideas for designing efficient and accurate numerical methods for the NLSE (1.1) with dark/bright solitons in previous sections can be easily extended to NLSE with general nonlinearity and/or external potential and coupled nonlinear Schrödinger equations (NLSEs) arising from pulse propagation in multi-mode fibers [29,30,14], multi-component Bose–Einstein condensates [9], etc.

5.1. Numerical methods for NLSE with general nonlinearity and/or external potential

Consider the following NLSE with general nonlinearity and/or external potential

$$i\partial_t\psi(x,t) = -\frac{1}{2}\partial_{xx}\psi(x,t) + V(x)\psi(x,t) + f(|\psi(x,t)|^2)\psi(x,t), \quad x\in\mathbb{R}, \quad t>0, \tag{5.1}$$

where $V(x)$ is a given real-valued external potential and $f(\rho)$ is a given real-valued general nonlinearity satisfying $f(0)=0$. Typical examples include $f(\rho)=\beta\rho$ for cubic nonlinearity, $f(\rho)=\beta\rho+\gamma\rho^2$ for cubic-quintic nonlinearity [16], and $f(\rho)=\frac{\beta\rho}{1+\gamma\rho}$ [32] with β and γ given real constants.

If $V(x)\to+\infty$ when $|x|\to\infty$ in (5.1), e.g. harmonic oscillator potential, due to mass and energy conservation, in general, the initial data ψ_0 in (1.12) and the solution ψ of (5.1) with (1.12) need satisfy

$$\psi(x,t)\to 0, \quad |x|\to\infty, \quad t\geqslant 0.$$

Then the NLSE (5.1) with (1.12) can be truncated and approximated on $\Omega=[L_1,L_2]$ with periodic or homogeneous Dirichlet or Neumann boundary conditions. The truncated problem can be numerically solved via TSFP or TSSP or TSCP methods similar to those in Section 4 and the details are omitted here for brevity. For example, for the TSSP method, we need only replace the first and third steps in (4.8) by

$$\psi_j^{(1)} = e^{-i[V(x_j)+f(|\psi_j^n|^2)]\tau/2}\psi_j^n, \quad \psi_j^{n+1} = e^{-i[V(x_j)+f(|\psi_j^{(2)}|^2)]\tau/2}\psi_j^{(2)}.$$

Now we assume $V(x)\to V_0$ when $|x|\to\infty$ in (5.1) with V_0 a given constant. If the initial data in (1.12) satisfies (4.1), such as dynamics and/or interaction of bright solitons, the NLSE (5.1) with (1.12) can be truncated and approximated on $\Omega=[L_1,L_2]$ with periodic or homogeneous Dirichlet or Neumann boundary conditions. The truncated problem can be numerically solved via TSFP or TSSP or TSCP methods similar to those in Section 4 and the details are omitted here for brevity. Similarly, if the initial data in (1.12) satisfies (3.1), such as dynamics and/or interaction of type I dark solitons, the NLSE (5.1) with (1.12) can be truncated and approximated on $\Omega=[L_1,L_2]$ with homogeneous Neumann boundary conditions. Then the truncated problem can be numerically solved via TSCP or TSFD methods similar as those in Section 3 and the details are omitted here for brevity. Finally, if the initial data in (1.12) satisfies (2.1), such as dynamics and/or interaction of type II dark solitons, then we need to introduce the transformation (2.19) to 'rest' the highly oscillatory phase background at far field. Similar to those in Section 2.2, plugging the transformation (2.19) into (5.1), we obtain

$$i\partial_t\phi(x,t) = -\frac{1}{2}\partial_{xx}\phi - ik\partial_x\phi + \frac{1}{2}k^2\phi + V(x)\phi + f(|\phi|^2)\phi, \quad x\in\mathbb{R}, \quad t>0.$$

This problem can be truncated on an interval $\Omega=[L_1,L_2]$ with homogeneous Neumann boundary condition. Then the truncated problem can be numerically solved by the TSFD method similar to (2.34) and the details are omitted for brevity.

5.2. Numerical methods for coupled NLSEs

To simplify the presentation, here we only show the case of coupled NLSEs with two equations

$$i\partial_t\psi_1(x,t) = -\frac{1}{2}\partial_{xx}\psi_1 + V_1(x)\psi_1 + f_1(|\psi_1|^2,|\psi_2|^2)\psi_1, \tag{5.2}$$

$$i\partial_t\psi_2(x,t) = -\frac{1}{2}\partial_{xx}\psi_2 + V_2(x)\psi_2 + f_2(|\psi_1|^2,|\psi_2|^2)\psi_2, \quad x\in\mathbb{R}, \quad t>0, \tag{5.3}$$

where $V_1(x)$ and $V_2(x)$ are given real-valued external potentials, $f_1(\rho_1,\rho_2)$ and $f_2(\rho_1,\rho_2)$ are two given real-valued functions satisfying $f_1(0,0)=0$ and $f_2(0,0)=0$. The corresponding initial data are given as

$$\psi_1(x,0)=\psi_1^{(0)}(x), \quad \psi_2(x,0)=\psi_2^{(0)}(x), \quad x\in\mathbb{R}. \tag{5.4}$$

A typical example for the nonlinearities and external potentials are given as [29,30,9]

$$V_1(x)=V_2(x)\equiv 0, \quad f_1(\rho_1,\rho_2)=\beta_{11}\rho_1+\beta_{12}\rho_2, \quad f_2(\rho_1,\rho_2)=\beta_{21}\rho_1+\beta_{22}\rho_2, \quad 0\leqslant\rho_1,\rho_2<\infty; \tag{5.5}$$

where $\beta_{11},\beta_{12},\beta_{21}$ and β_{22} are given real constants.

We first assume $V_1(x)\to V_1^0$ and $V_2(x)\to V_2^0$ when $|x|\to\infty$ in (5.2) with V_1^0 and V_2^0 two given constants. If the initial data in (5.4) satisfies

$$\psi_1^{(0)}(x)\to 0, \quad \psi_2^{(0)}(x)\to 0, \quad x\to\pm\infty,$$

such as interactions between bright–bright (B–B) solitons, the original problem can be truncated and approximated on $\Omega=[L_1,L_2]$ with periodic or homogeneous Dirichlet or Neumann boundary conditions. Then the truncated problem can be numerically solved via TSFP or TSSP or TSCP methods similar to those in Section 4 and the details are omitted here for brevity.

If the initial data in (5.4) satisfies

$$\psi_1^{(0)}(x) \to A_\pm^0, \quad \psi_2^{(0)}(x) \to B_\pm^0, \quad x \to \pm\infty,$$

with $A_\pm^0$ and $B_\pm^0$ given constants, such as interactions between two type I dark solitons (D1-D1, e.g. $A_+^0 \neq A_-^0$ and $B_+^0 \neq B_-^0$) or type I dark–bright solitons (D1-B, e.g. $A_+^0 = A_-^0 = 0$ or $B_+^0 = B_-^0 = 0$), the original problem can be truncated and approximated on $\Omega = [L_1, L_2]$ with homogeneous Neumann boundary conditions. Then the truncated problem can be numerically solved via TSCP or TSFD methods similar as those in Section 3 and the details are omitted here for brevity.

Finally, if the initial data in (5.4) satisfies

$$\psi_1^{(0)}(x) \to A_\pm^0 e^{ik_1 x}, \quad \psi_2^{(0)}(x) \to B_\pm^0 e^{ik_2 x}, \quad x \to \pm\infty,$$

with $k_1, k_2, A_\pm^0$ and $B_\pm^0$ given constants, such as interactions between two type II dark solitons (D2–D2, e.g. $k_1 \neq 0, k_2 \neq 0$, $A_+^0 \neq A_-^0$ and $B_+^0 \neq B_-^0$) or type II dark-type I dark solitons (D2–D1, e.g. $A_+^0 \neq A_-^0, B_+^0 \neq B_-^0$ and $k_1 \neq 0, k_2 = 0$ or $k_1 = 0, k_2 \neq 0$) or type II dark–bright solitons (D2-B, e.g. $A_+^0 \neq A_-^0, k_1 \neq 0$ and $B_+^0 = B_-^0 = 0$ or $B_+^0 \neq B_-^0, k_2 \neq 0$ and $A_+^0 = A_-^0 = 0$), then we need to introduce the following transformations to 'rest' the highly oscillatory phase background at far field

$$\phi_1(x,t) = \psi_1(x,t)e^{-ik_1 x} \Longleftrightarrow \psi_1(x,t) = \phi_1(x,t)e^{ik_1 x}, \quad x \in \mathbb{R}, \quad t \geqslant 0, \tag{5.6}$$

if $A_+^0 \neq A_-^0$ and $k_1 \neq 0$, and/or

$$\phi_2(x,t) = \psi_2(x,t)e^{-ik_2 x} \Longleftrightarrow \psi_2(x,t) = \phi_2(x,t)e^{ik_2 x}, \quad x \in \mathbb{R}, \quad t \geqslant 0, \tag{5.7}$$

if $B_+^0 \neq B_-^0$ and $k_2 \neq 0$. Similar to those in section 2.2, plugging the transformations (5.6) and/or (5.7) into the coupled NLSEs (5.2)–(5.4), we obtain a truncated and approximated problem for ϕ_1 and ϕ_2 on an interval $\Omega = [L_1, L_2]$ with homogeneous Neumann boundary condition. Finally, we can numerically solve the truncated problem by the TSFD method similar to (2.34) and the details are omitted for brevity.

Of course, if either $V_1(x) \to \infty$ or $V_2(x) \to \infty$ when $|x| \to \infty$ in (5.2)–(5.3), we can extend the ideas and methods in Section 5.1 straightforward and the details are omitted for brevity.

5.3. Numerical results

Here we report some preliminary results on interactions of dark/bright solitons in coupled NLSEs by our numerical methods. In order to do so, the initial data in (5.4) and parameters in (5.2)–(5.5) for different cases are taken as.

- I. Interaction between two type II dark solitons (D2–D2) with $\beta_{11} = \beta_{12} = \beta_{21} = \beta_{22} = 1$ and

  $$\psi_1^{(0)}(x) = [a_1 \tanh(a_1(x - x_1)) + i(v_1 - k_1)]e^{ik_1 x},$$
  $$\psi_2^{(0)}(x) = [a_2 \tanh(a_2(x - x_2)) + i(v_2 - k_2)]e^{ik_2 x}, \quad x \in \mathbb{R};$$

- II. Interaction between type II dark and type I dark solitons (D2–D1) with $\beta_{11} = \beta_{12} = \beta_{21} = \beta_{22} = 1$ and

  $$\psi_1^{(0)}(x) = [a_1 \tanh(a_1(x - x_1)) + i(v_1 - k_1)]e^{ik_1 x}, \quad \psi_2^{(0)}(x) = a_2 \tanh(a_2(x - x_2)) + iv_2;$$

- III. Interaction between type II dark and bright solitons (D2–B) with $\beta_{11} = \beta_{12} = \beta_{21} = 1, \beta_{22} = -1$ and

  $$\psi_1^{(0)}(x) = [a_1 \tanh(a_1(x - x_1)) + i(v_1 - k_1)]e^{ik_1 x}, \quad \psi_2^{(0)}(x) = a_2 \mathrm{sech}(a_2(x - x_2))e^{iv_2 x};$$

- IV. Interaction between type I dark and bright solitons (D1–B) with $\beta_{11} = \beta_{12} = \beta_{21} = 1, \beta_{22} = -1$ and

  $$\psi_1^{(0)}(x) = a_1 \tanh(a_1(x - x_1)) + iv_1, \quad \psi_2^{(0)}(x) = a_2 \mathrm{sech}(a_2(x - x_2))e^{iv_2 x};$$

- V. Interaction between two bright solitons (B–B) with $\beta_{11} = \beta_{12} = \beta_{21} = \beta_{22} = -1$ and

  $$\psi_1^{(0)}(x) = a_1 \mathrm{sech}(a_1(x - x_1))e^{iv_1 x}, \quad \psi_2^{(0)}(x) = a_2 \mathrm{sech}(a_2(x - x_2))e^{iv_2 x}, \quad x \in \mathbb{R}.$$

Figs. 5.1–5.5 display time evolution of $|\psi_1|$ and $|\psi_2|$ for the above 5 cases, respectively.

From Figs. 5.1–5.5 and additional results not shown here for brevity, we can draw the following observations for the interactions of dark/bright solitons in coupled NLSEs: (i) The two solitons in all cases are transmitted through each other without any oscillation in the collision region. (ii) In the D2–D2 interaction, the one of large amplitude moves without radiation while the other one with some small radiation. (ii) In the D2–D1 interaction, both the two dark solitons emit new small waves during propagation. Moreover, the type I dark soliton seems to be dragged deeper and deeper into the background (or namely become darker and darker) while the minima of the type II dark soliton stays unchange. (iii) In the D2–B interaction, the type II dark soliton does while the bright soliton does not emit new small waves during propagation. (iv) In the D1–B interaction, the bright soliton will become thinner and move slower during propagation, meanwhile there will be a small wave created in the type I dark soliton, which moves in the same direction as the bright soliton. It looks like that the type

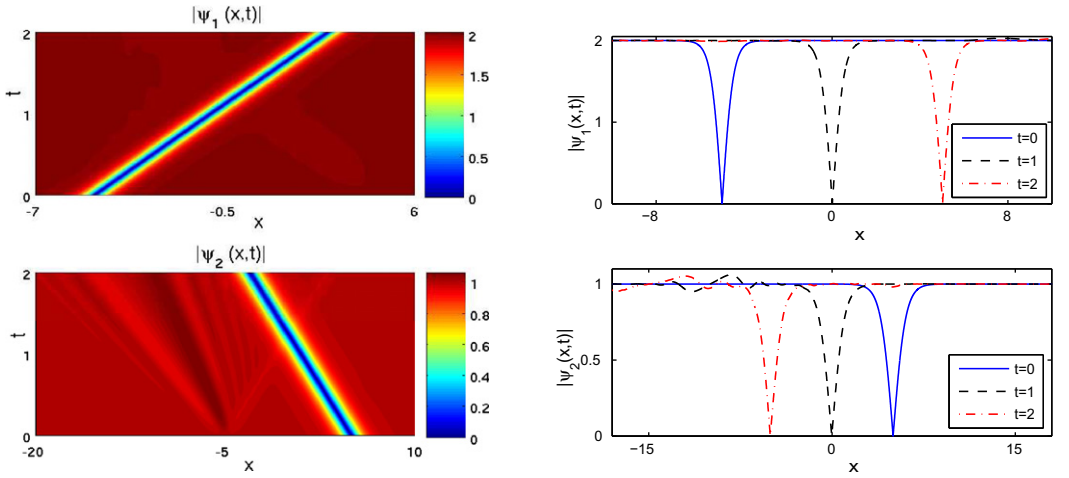

Fig. 5.1. Time evolution of $|\psi_1|$ and $|\psi_2|$ for the interaction between two type II dark solitons (D2-D2), i.e. case I, with $a_1 = 2,\ k_1 = 5,\ v_1 = 5,\ x_1 = -5,\ a_2 = 1,\ k_2 = -5,\ v_2 = -5$ and $x_2 = 5$.

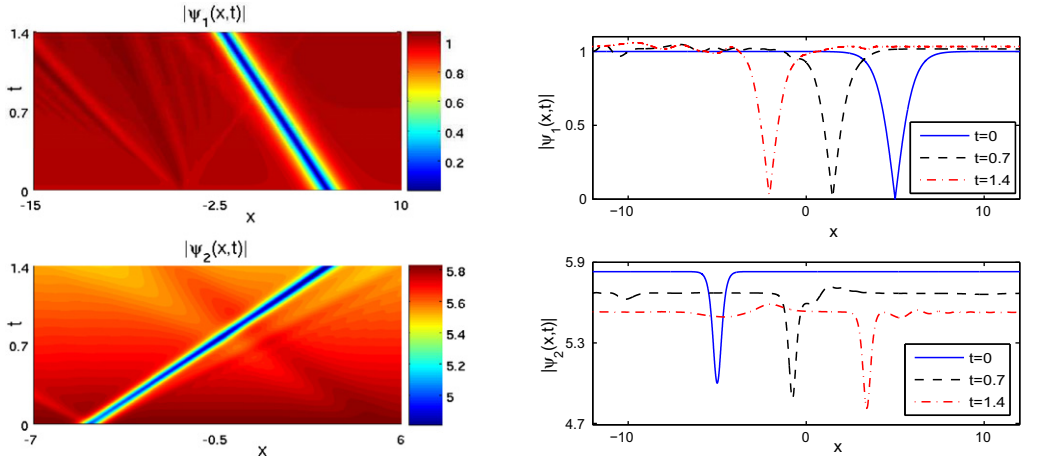

Fig. 5.2. Time evolution of $|\psi_1|$ and $|\psi_2|$ for the interaction between type II dark and type I dark solitons (D2-D1), i.e. case II, with $a_1 = 1,\ k_1 = 5,\ v_1 = -5,\ x_1 = 5,\ a_2 = 3,\ v_2 = 5$ and $x_2 = -5$.

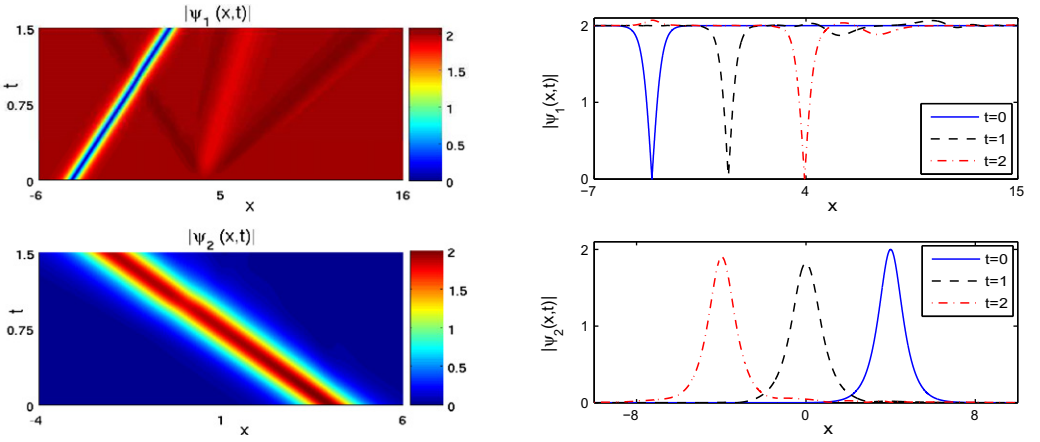

Fig. 5.3. Time evolution of $|\psi_1|$ and $|\psi_2|$ for the interaction between type II dark and bright solitons (D2-B), i.e. case III, with $a_1 = 2,\ k_1 = 4,\ v_1 = 4,\ x_1 = -4,\ a_2 = 2,\ v_2 = -4$ and $x_2 = 4$.

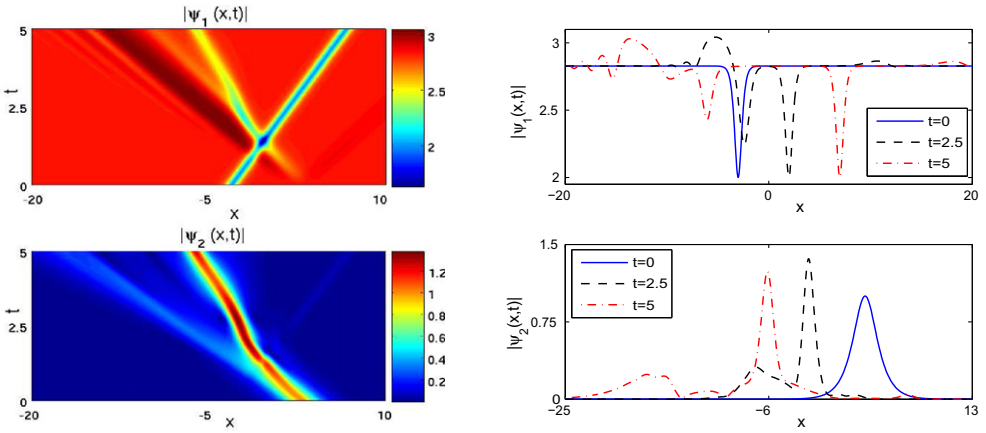

Fig. 5.4. Time evolution of $|\psi_1|$ and $|\psi_2|$ for the interaction between type I dark and bright solitons (D1-B), i.e. case IV, with $a_1 = 2,\ \nu_1 = 2,\ x_1 = -3,\ a_2 = 1,\ \nu_2 = -3$ and $x_2 = 3$.

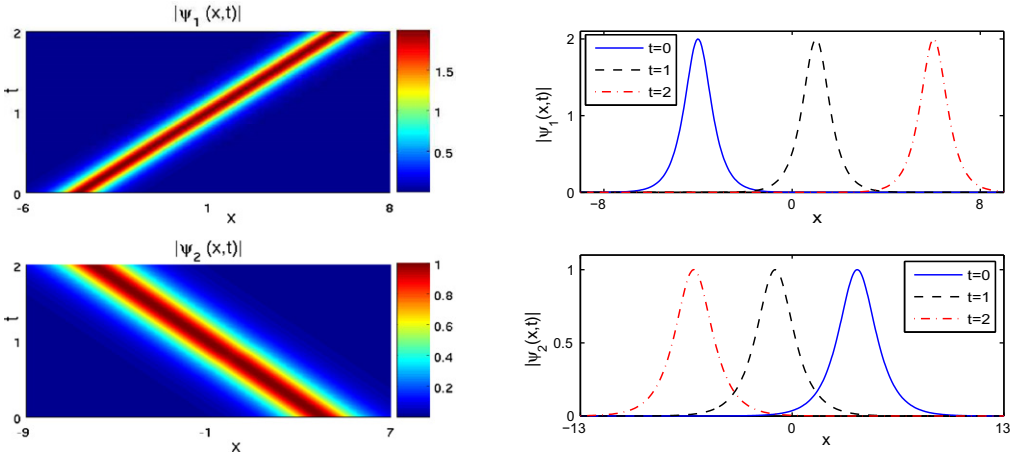

Fig. 5.5. Time evolution of $|\psi_1|$ and $|\psi_2|$ for the interaction between two bright solitons (B–B), i.e. case V, with $a_1 = 2,\ \nu_1 = 5,\ x_1 = -4,\ a_2 = 1,\ \nu_2 = -5$ and $x_2 = 4$.

I dark soliton 'split' a small piece of the bright soliton. (v) In the B–B interaction, the two bright solitons keep their shapes and velocity, and there is no radiation emitted during propagation.

In a subsequent paper [39], extensive numerical studies will be carried out for interactions of dark/bright solitions in NLSE with general nonlinearity and/or external potential and vector solitons in coupled NLSEs.

6. Conclusion

New efficient and accurate numerical methods were presented for simulating the nonlinear Schrödinger equation (NLSE) when the initial data has non-rest or highly oscillatory phase background at far field, such as type II dark soliton solutions, based on either designing accurate and simple artificial boundary conditions or introducing a proper transformation to rest the highly oscillatory phase background. Comparisons between these numerical methods were carried out when the NLSE admits type II dark solition solutions. Moreover, various existing numerical methods were reviewed and compared for computing the NLSE when the initial data has nonzero rest background at far field such as type I dark solitons or decays to zero at far field such as bight solitions. Based on our extensive numerical comparison results, in order to solve the NLSE numerically, we suggest that: (a) If the initial data has non-rest or highly oscillatory phase background at far field, e.g. type II dark solitons and their interactions, then the time-splitting finite difference through a transformation (TSFD-T) method (2.34) with (2.35) and (2.27) is the most efficient and accurate numerical method; (b) if the initial data has non-zero rest background at far field, e.g. type I dark solitons and their interactions, then the time-splitting cosine pseudospectral (TSCP) method (3.9) is the most efficient and accurate numerical method; and (c) if the initial data decays to zero at far field, e.g. bright solitons and their interactions, then either the time-splitting cosine pseudospectral (TSCP) method (3.9), or time-splitting sine

pseudospectral (TSSP) method (4.8), or time-splitting Fourier pseudospectral (TSFP) method (4.9) is the most efficient and accurate numerical method. In addition, these numerical methods were extended to solve the NLSE with general nonlinearity and/or external potential and the coupled nonlinear Schrödinger equations (NLSEs) with vector solitons and their interactions. Finally, we applied these efficient and accurate numerical methods for studying numerically stability and interactions of type II dark solitons, type I dark solitons and bright solitons of NLSE and interactions of vector solitons of coupled NLSEs. Based on the numerical results, we can conclude that: (i) All the bright, type I dark and type II dark solitons are dynamically stable in NLSE under the small perturbation at the initial data. (ii) In general, the interactions for all the three solitons are elastic and they keep their velocity and shape before and after collision. (iii) For the interaction of two type I dark solitons or two type II dark soltions, when the velocities are less than a critical value, they will be repulsed by each other; otherwise they will be transmitted through each other. (iv) Soltons wings will be created at collision time and disappear after collision for bright-bright solitons interaction, and respectively, there is no soliton wings created throughout the whole process of interaction for dark–dark solitons interaction. We remark that the numerical methods and the ideas for designing them can be extended to three-wave interactions in nonlinear optics [14] and spin-1 Bose–Einstein condensation [12].

Acknowledgements

This work was supported by the Singapore A*STAR SERC "Complex Systems" Research Programme grant R-146-000-171-305 and the Academic Research Fund of Ministry of Education of Singapore grant R-146-000-120-112. Part of this work was done when the first author was visiting Beijing Computational Science Research Center in 2011. We also thank Dr. Xuanchun Dong for stimulating discussion.

Appendix A. Proof of Lemma 2.1

Proof. Differentiating (2.9) with respect to t, noticing (2.6) and (2.7), and integration by parts, we have

$$\begin{aligned} N_1'(t) &= \int_{L_1}^{L_2} (\psi_t\bar{\psi} + \psi\bar{\psi}_t)dx + k\Big[|\psi(L_2,t)|^2 - |\psi(L_1,t)|^2\Big] = i\int_{L_1}^{L_2} [(-i\bar{\psi}_t)\psi - (i\psi_t)\bar{\psi}]dx + k\Big[|\psi(L_2,t)|^2 - |\psi(L_1,t)|^2\Big] \\ &= -\mathrm{Im}\big[\bar{\psi}(L_2,t)\partial_x\psi(L_2,t) - \bar{\psi}(L_1,t)\partial_x\psi(L_1,t)\big] + k\Big[|\psi(L_2,t)|^2 - |\psi(L_1,t)|^2\Big] \\ &= -k\Big[|\psi(L_2,t)|^2 - |\psi(L_1,t)|^2\Big] + k\Big[|\psi(L_2,t)|^2 - |\psi(L_1,t)|^2\Big] = 0, \quad t \geqslant 0, \end{aligned} \tag{A.1}$$

which immediately implies the conservation of the modified mass in (2.11). Similarly, differentiating (2.10) with respect to t, we get

$$\begin{aligned} E_1'(t) &= \frac{1}{2}\int_{L_1}^{L_2} \partial_t[|\psi_x|^2 + \beta|\psi|^4]dx + k\mathrm{Im}\big[\psi(L_2,t)\partial_t\bar{\psi}(L_2,t) - \psi(L_1,t)\partial_t\bar{\psi}(L_1,t)\big] \\ &= \int_{L_1}^{L_2} \left[\left(-\frac{1}{2}\bar{\psi}_{xx} + \beta|\psi|^2\bar{\psi}\right)\psi_t + \left(-\frac{1}{2}\psi_{xx} + \beta|\psi|^2\psi\right)\bar{\psi}_t\right]dx + \mathrm{Re}\big[\psi_t(L_2,t)\bar{\psi}_x(L_2,t) - \psi_t(L_1,t)\bar{\psi}_x(L_1,t)\big] \\ &\quad + k\mathrm{Im}\big[\psi(L_2,t)\partial_t\bar{\psi}(L_2,t) - \psi(L_1,t)\partial_t\bar{\psi}(L_1,t)\big] \\ &= 0, \quad t \geqslant 0, \end{aligned} \tag{A.2}$$

which implies the conservation of the modified energy in (2.11). □

Appendix B. Proof of Lemma 2.2

Proof. Multiplying (2.12) by $\bar{\psi}_j^{n+\frac{1}{2}} = \frac{1}{2}(\bar{\psi}_j^{n+1} + \bar{\psi}_j^n)$, and then subtracting the resulted equation from its conjugate, we get

$$2i\delta_t^+|\psi_j^n|^2 = \frac{1}{8}\Big[(\psi_j^{n+1} + \psi_j^n)\delta_x^2(\bar{\psi}_j^{n+1} + \bar{\psi}_j^n) - (\bar{\psi}_j^{n+1} + \bar{\psi}_j^n)\delta_x^2(\psi_j^{n+1} + \psi_j^n)\Big], \quad 0 \leqslant j \leqslant N. \tag{B.1}$$

Taking summation of $\delta_t^+(|\psi_j^n|^2 + |\psi_j^{n+1}|^2)$ for $0 \leqslant j \leqslant N-1$, summation by parts, noticing (B.1) and (2.13), we have

$$\delta_t^+\sum_{j=0}^{N-1}\Big(|\psi_j^n|^2 + |\psi_{j+1}^n|^2\Big) = -\frac{2k}{h}\Big(|\psi_N^{n+\frac{1}{2}}|^2 - |\psi_0^{n+\frac{1}{2}}|^2\Big) = -\frac{2k\tau}{h}\delta_t^+\sum_{l=1}^{n}\Big(|\psi_N^{l-\frac{1}{2}}|^2 - |\psi_0^{l-\frac{1}{2}}|^2\Big). \tag{B.2}$$

This, together with (2.16), implies

$$N_1^{n+1} = \frac{h}{2}\sum_{j=0}^{N-1}\Big(|\psi_j^{n+1}|^2 + |\psi_{j+1}^{n+1}|^2\Big) + k\tau\sum_{l=1}^{n+1}\Big(|\psi_N^{l-\frac{1}{2}}|^2 - |\psi_0^{l-\frac{1}{2}}|^2\Big) = \frac{h}{2}\sum_{j=0}^{N-1}\Big(|\psi_j^n|^2 + |\psi_{j+1}^n|^2\Big) + k\tau\sum_{l=1}^{n}\Big(|\psi_N^{l-\frac{1}{2}}|^2 - |\psi_0^{l-\frac{1}{2}}|^2\Big) = N_1^n, \quad n \geqslant 0.$$

Thus the mass conservation in (2.18) of CNFD method (2.12) can be obtained by induction.

Similarly, multiplying (2.12) by $\delta_t^+\bar{\psi}_j^n$, and then adding the resulted equation with its conjugate, we get

$$\frac{\beta}{2}\delta_t^+|\psi_j^n|^4 = \frac{1}{2}\left(\delta_x^2\psi_j^{n+\frac{1}{2}}\delta_t^+\bar{\psi}_j^n + \delta_x^2\bar{\psi}_j^{n+\frac{1}{2}}\delta_t^+\psi_j^n\right), \quad j = 0,\ldots,N. \tag{B.3}$$

Taking summation of $\delta_t^+(|\psi_j^n|^4 + |\psi_{j+1}^n|^4)$ for $0 \leqslant j \leqslant N-1$, summation by parts, noticing (B.3) and (2.13), we have

$$\begin{aligned}\frac{\beta}{2}\delta_t^+\sum_{j=0}^{N-1}(|\psi_j^n|^4 + |\psi_{j+1}^n|^4) &= -\sum_{j=0}^{N-1}\delta_t^+|\delta_x^+\psi_j^n|^2 - \frac{2k}{h}\mathrm{Im}\left[\psi_N^{n+\frac{1}{2}}\delta_t^+\bar{\psi}_N^n - \psi_0^{n+\frac{1}{2}}\delta_t^+\bar{\psi}_0^n\right]\\ &= -\sum_{j=0}^{N-1}\delta_t^+|\delta_x^+\psi_j^n|^2 - \frac{2k\tau}{h}\delta_t^+\sum_{l=1}^{n}\mathrm{Im}\left[\psi_N^{l-\frac{1}{2}}\delta_t^+\bar{\psi}_N^{l-1} - \psi_0^{l-\frac{1}{2}}\delta_t^+\bar{\psi}_0^{l-1}\right].\end{aligned}$$

This, together with (2.17), implies

$$\begin{aligned}E_1^{n+1} &= \frac{h}{2}\sum_{j=0}^{N-1}\left[|\delta_x^+\psi_j^{n+1}|^2 + \frac{\beta}{2}\left(|\psi_j^{n+1}|^4 + |\psi_{j+1}^{n+1}|^4\right)\right] + k\tau\mathrm{Im}\sum_{l=1}^{n+1}\left[\psi_N^{l-\frac{1}{2}}\delta_t^+\bar{\psi}_N^{l-1} - \psi_0^{l-\frac{1}{2}}\delta_t^+\bar{\psi}_0^{l-1}\right]\\ &= \frac{h}{2}\sum_{j=0}^{N-1}\left[|\delta_x^+\psi_j^n|^2 + \frac{\beta}{2}\left(|\psi_j^n|^4 + |\psi_{j+1}^n|^4\right)\right] + k\tau\mathrm{Im}\sum_{l=1}^{n}\left[\psi_N^{l-\frac{1}{2}}\delta_t^+\bar{\psi}_N^{l-1} - \psi_0^{l-\frac{1}{2}}\delta_t^+\bar{\psi}_0^{l-1}\right] = E_1^n.\end{aligned}$$

Again, the energy conservation in (2.18) of CNFD method (2.12) can be obtained by induction. □

References

[1] F. Abdullaev, S. Darmanyan, P. Khabibullaev, Optical Solitons, Springer Verlag, New York, 1993.
[2] M.J. Ablowitz, H. Segur, Solitons and the Inverse Scattering Transform, SIAM, Philadelphia, 1981.
[3] G.D. Akrivis, Finite difference discretization of the cubic Schrödinger equation, IMA J. Numer. Anal. 13 (1993) 115–124.
[4] G.D. Akrivis, V.A. Dougalis, O. Karakashian, Solving the systems of equations arising in the discretization of some nonlinear PDEs by implicit Runge–Kutta methods, RAIRO Model. Math. Anal. Numer. 31 (1997) 251–287.
[5] M.H. Anderson, J.R. Ensher, M.R. Matthews, C.E. Wieman, E.A. Cornell, Observation of Bose–Einstein condensation in a dilute atomic vapor, Science 269 (1995) 198–201.
[6] X. Antoine, A. Arnold, C. Besse, M. Ehrhardt, A. Schädle, A review of transparent and artificial boundary condition techniques for linear and nonlinear Schrödinger equations, Commun. Comput. Phys. 4 (2008) 729–796.
[7] X. Antoine, C. Besse, P. Klein, Absorbing boundary conditions for general nonlinear Schrödinger equations, SIAM J. Sci. Comput. 33 (2011) 1008–1033.
[8] W. Bao, Numerical methods for the nonlinear Schrödinger equation with nonzero far-field conditions, Methods Appl. Anal. 11 (2004) 367–387.
[9] W. Bao, Ground states and dynamics of multi-component Bose–Einstein condensates, Multiscale Model. Simul. 2 (2004) 210–236.
[10] W. Bao, D. Jaksch, P.A. Markowich, Numerical solution of the Gross–Pitaevskii equation for Bose–Einstein condensation, J. Comput. Phys. 187 (2003) 318–342.
[11] W. Bao, S. Jin, P.A. Markowich, On time-splitting spectral approximations for the Schrödinger equation in the semiclassical regime, J. Comput. Phys. 175 (2002) 487–524.
[12] W. Bao, F.Y. Lim, Computing ground states of spin-1 Bose–Einstein condensates by the normalized gradient flow, SIAM J. Sci. Comput. 30 (2008) 1925–1948.
[13] W. Bao, Y. Zhang, Dynamics of the ground state and central vortex states in Bose–Einstein condensation, Math. Models Meth. Appl. Sci. 15 (2005) 1863–1896.
[14] W. Bao, C. Zheng, A time-splitting spectral method for three-wave interactions in media with competing quadratic and cubic nonlinearities, Commun. Comput. Phys. 2 (2007) 123–140.
[15] I.V. Barashenkov, A.O. Harin, Nonrelativistic Cherns–Simons theory for the repulsive Bose gas, Phys. Rev. Lett. 72 (1994) 1575–1579.
[16] I.V. Barashenkov, E.Y. Panova, Stability and evolution of the quiescent and travelling solitonic bubbles, Physica D 69 (1993) 114–134.
[17] C. Besse, B. Bidegaray, S. Descombes, Order estimates in time of splitting methods for the nonlinear Schrödinger equation, SIAM J. Numer. Anal. 40 (2002) 26–40.
[18] L.D. Carr, J.N. Kutz, W.P. Reinhardt, Stability of stationary states in the cubic nonlinear Schrödinger equation: applications to the Bose–Einstein condensate, Phys. Rev. E 63 (2001) 066604.
[19] R. Carretero-González, D.J. Frantzeskakis, P.G. Kevrekidis, Nonlinear waves in Bose–Einstein condensates: physical relevance and mathematical techniques, Nonlinearity 21 (2008) 139–202.
[20] Q.S. Chang, E. Jia, W. Sun, Difference schemes for solving the generalized nonlinear Schrödinger equation, J. Comput. Phys 148 (1999) 397–415.
[21] T. Dauxois, M. Peyrard, Physics of Solitons, Cambridge University Press, 2006.
[22] M. Delfour, M. Fortin, G. Payre, Finite-difference solutions of a nonlinear Schrödinger equation, J. Comput. Phys. 44 (1981) 277–288.
[23] D.J. Frantzeskakis, Dark solitons in atomic Bose–Einstein condensates: from theory to experiments, J. Phys. A Math. Theor. 43 (2010) 213001.
[24] D.F. Griffiths, A.R. Mitchell, J.L. Morris, A numerical study of the nonlinear Schrödinger equation, Comput. Methods Appl. Mech. Eng. 45 (1984) 177–215.
[25] A. Hasegawa, F. Tappert, Transmission of stationary nonlinear optical pulses in dispersive dielectric fibers: I. Anomalous dispersion, Appl. Phys. Lett. 23 (1973) 142–144.
[26] A. Hasegawa, F. Tappert, Transmission of stationary nonlinear optical pulses in dispersive dielectric fibers: II. Normal dispersion, Appl. Phys. Lett. 23 (1973) 171–172.
[27] H. Han, Z. Huang, Exact artificial boundary conditions for Schrödinger equation in $\mathbb{R}^2$, Commun. Math. Sci. 2 (2004) 79–94.
[28] O. Karakashian, G.D. Akrivis, V.A. Dougalis, On optimal order error estimates for the nonlinear Schrödinger equation, SIAM J. Numer. Anal. 30 (1993) 377–400.
[29] Y.S. Kivshar, B. Luther-Davies, Dark optical solitons: physics and applications, Phys. Rep. 298 (1998) 81–197.
[30] Y.S. Kivshar, X. Yang, Perturbation-induced dynamics of dark solitons, Phys. Rev. E 49 (1994) 1657–1670.
[31] P. Muruganandam, S.K. Adhikari, Fortran programs for the time-dependent Gross–Pitaevskii equation in a fully anisotropic trap, Comput. Phys. Commun. 180 (2009) 1888–1912.
[32] A.C. Newell, Solitons in Mathematics and Physics, SIAM, Philadelphia, 1985.

[33] S. Novikov, S.V. Manakov, L.P. Pitaevskij, V.E. Zakharov, Theory of Solitons: The Inverse Scattering Methods, Plenum, New York, 1984.
[34] J.S. Russell, Report on waves, in: Fourteenth Meeting of the British Association for the Advancement of Science, 1844.
[35] A.B. Shamardan, The numerical treatment of the nonlinear Schrödinger equation, Comput. Math. Appl. 19 (1990) 67–73.
[36] J. Shen, T. Tang, Spectral and High-Order Methods with Applications, Science, Beijing, 2006.
[37] G. Strang, On the construction and comparison of difference schemes, SIAM J. Numer. Anal. 5 (1968) 505–517.
[38] T.R. Taha, M.J. Ablowitz, Analytical and numerical aspects of certain nonlinear evolution equations: II. Numerical, nonlinear Schrodinger equation, J. Comput. Phys. 55 (1984) 203–230.
[39] Q. Tang, Dynamics and interaction of the multi-component solitons in coupled nonlinear Schrödinger equations, in preparation.
[40] I.M. Uzunov, V.S. Gerdjikov, Self-frequency shift of dark solitons in optical fibers, Phys. Rev. A 47 (1993) 1582–1585.
[41] D. Vudragovic, I. Vidanovic, A. Balaz, P. Muruganandam, S.K. Adhikari, C programs for solving the time-dependent Gross–Pitaevskii equation in a fully anisotropic trap, Comput. Phys. Commun. 183 (2012) 2021–2025.
[42] J.A.C. Weideman, B.M. Herbst, Split-step methods for the solution of the nonlinear Schrödinger equation, SIAM J. Numer. Anal. 23 (1986) 485–507.
[43] V.E. Zakharov, A.B. Shabat, Exact theory of two-dimensional self-focusing and one-dimensional self-modulation of waves in nonlinear media, Sov. Phys. JETP 34 (1972) 62–69.
[44] V.E. Zakharov, A.B. Shabat, Interaction between solitons in a stable medium, Sov. Phys. JETP 37 (1973) 823–828.
[45] C. Zheng, Exact nonreflecting boundary conditions for one-dimensional cubic nonlinear Schrödinger equations, J. Comput. Phys. 215 (2006) 552–562.
[46] G. Zouraris, On the convergence of a linear two-step finite element method for the nonlinear Schrödinger equation, M2AN Math. Model. Numer. Anal. 35 (2001) 389–405.